Huntingtin phosphorylation governs BDNF homeostasis and improves the phenotype of Mecp2 knockout mice

Yann Ehinger*[1], Julie Bruyère*[2], Nicolas Panayotis[1], Yah-Se Abada[3], Emilie Borloz[1], Valérie Matagne[1], Chiara Scaramuzzino[2], Hélène Vitet[2], Benoit Delatour[3], Lydia Saidi[1], Laurent Villard[1], Frédéric Saudou[2,#], Jean-Christophe Roux[1,#].

[1]Aix Marseille Univ, INSERM, MMG, UMR_S 1251, 13385. Marseille, France

[2]Univ. Grenoble Alpes, Inserm, U1216, CHU Grenoble Alpes, Grenoble Institut Neurosciences, GIN, F-38000 Grenoble, France.

[3]Sorbonne Université, Institut du Cerveau et de la Moelle épinière, ICM, Inserm U1127, CNRS UMR 7225, F-75013, Paris, France

*Equal contributions

[#]Corresponding authors: frederic.saudou@inserm.fr (F.S.; https://orcid.org/0000-0001-6107-1046 or jean-christophe.roux@univ-amu.fr (J.C.R.)

Present address for Y.E.: Department of Neurology, University of California, San Francisco, San Francisco, CA 94143, USA

Present address for N.P.: Department of Biomolecular Sciences, Weizmann Institute of Science, Rehovot 7610001, Israel.

Present address for L.S.: Department of Psychiatry and Neuroscience, Faculty of medicine, Centre de recherche CERVO, Université Laval, 2601, Canardière, Room F-6500, Quebec City, QC, Canada

Keywords: Mecp2, Rett, BDNF, huntingtin (HTT), axonal transport

Abstract

Mutations in the X-linked *MECP2* gene are responsible for Rett syndrome (RTT), a severe neurological disorder for which there is no treatment. Several studies have linked the loss of MeCP2 function to alterations of brain-derived neurotrophic factor (BDNF) levels, but non-specific overexpression of BDNF only partially improves the phenotype of *Mecp2*-deficient mice. We and others have previously shown that huntingtin (HTT) scaffolds molecular motor complexes, transports BDNF-containing vesicles, and is under-expressed in *Mecp2* knock-out brains. Here we demonstrate that promoting HTT phosphorylation at Ser421, either by a phospho-mimetic mutation or inhibition of the phosphatase calcineurin, restores endogenous BDNF axonal transport *in vitro* in the corticostriatal pathway, increases striatal BDNF availability and synaptic connectivity *in vivo,* and improves the phenotype and the survival of *Mecp2* knockout mice—even though treatments were initiated only after the mice had already developed symptoms. Stimulation of endogenous cellular pathways may thus be a promising approach for the treatment of RTT patients.

Introduction

MeCP2 (Methyl CpG binding protein 2) is one of the most abundant proteins in the brain, yet the precise nature of its activities remains controversial. It was originally discovered as a DNA methylation-dependent transcriptional repressor (Meehan *et al*, 1992), but has also been shown to play various roles in chromatin compaction, global gene expression, alternative splicing, and miRNA processing (Skene *et al*, 2010; Chahrour *et al*, 2008; Young *et al*, 2005; Cheng *et al*, 2014). Interest in this protein rose sharply after it was discovered that mutations in *MECP2* cause Rett syndrome (RTT), a severe developmental disorder (Amir *et al*, 1999; Lyst & Bird, 2015). Females with RTT begin life apparently healthy, but between 6 and 18 months of age they undergo regression of early milestones, with deterioration of motor skills, eye contact, speech, and motor control; they then develop a range of neurological symptoms, including anxiety, respiratory dysrhythmias, and seizures (Lyst & Bird, 2015; Katz *et al*, 2016). Whereas loss of MeCP2 function leads to RTT, duplication or triplication of the locus lead to intellectual disability, autistic features, and motor dysfunction, as observed in males with *MECP2* duplication syndrome (Van Esch, 2012).

Disease-causing mutations in *MECP2* alter the expression of thousands of genes (Chahrour *et al*, 2008). Among these, brain-derived neurotrophic factor (BDNF), a neuronal modulator that plays a key role in neuronal survival, development, and plasticity (Cheng *et al*, 2011), is one of the best studied (Chang *et al*, 2006; Chen *et al*, 2003, 2015; Sampathkumar *et al*, 2016). BDNF appears to be involved in the appearance and progression of the RTT phenotype in mice: *Mecp2* knock-out mice (KO) present lower BDNF levels, and conditional BDNF deletion in *Mecp2* KO mice accelerates the onset of RTT-like symptoms (Chang *et al*, 2006). Conversely, conditional BDNF overexpression in the brain of *Mecp2* knock-out mice leads to an improvement of certain locomotor and electrophysiological deficits (Chang *et al*, 2006). Although it is possible that the incomplete rescue reflects that MeCP2 has much broader regulatory effects than BDNF, it is possible that BDNF overexpression fails to restore synaptic and neuronal function because it does not target the appropriate neurons. In support of this hypothesis, recent evidence suggests that MeCP2 deficiency leads to the disruption of cell-autonomous and autocrine BDNF signaling in excitatory glutamatergic neurons, and that increasing BDNF levels in diseased neurons restores their growth and ability to form synapses (Sampathkumar *et al*, 2016).

We have previously shown that BDNF homeostasis and transport involve huntingtin (HTT)

and HTT-associated protein 1 (Hap1) (Saudou & Humbert, 2016; Roux *et al*, 2012). Levels of both these proteins are lower than normal in excitatory cortical neurons deficient for *Mecp2* (Roux *et al*, 2012). Here we tested whether activating HTT, by a genetic or pharmacological approach, could improve BDNF homeostasis in *Mecp2*-deficient neuronal circuits and in *Mecp2* KO mice.

Results

BDNF transport is slowed in Mecp2-deficient axons

To examine BDNF transport in Mecp2-deficient neurons, we took advantage of the recent development and validation of microfluidic devices to reconstitute a neuronal network and monitor intracellular dynamics (Taylor *et al*, 2010; Virlogeux *et al*, 2018). We focused here on the corticostriatal network, which is altered in RTT and *Mecp2* KO mice (Roux *et al*, 2012; Xu *et al*, 2014). The device consists of a presynaptic compartment containing cortical neurons, a postsynaptic chamber containing striatal neurons, and a synaptic chamber containing corticostriatal contacts. Cortical neurons plated in the first compartment extend axons that connect to striatal dendrites within the synaptic compartment (Fig. 1A), thus creating an oriented corticostriatal network on-a-chip (Virlogeux *et al*, 2018). This network reproduces the physiological network as we previously showed that cortical neurons from embryonic day (E)15.5 are enriched in CTIP2/TBR1 neurons that correspond to the deepest layers of the cortex that send axons to the striatum. Also, most striatal neurons correspond to enkephalin-positive neurons that are the output-projecting neurons of the striatum (Virlogeux *et al*, 2018). Cortical neurons were transduced with mCherry-tagged BDNF lentivirus (BDNF-mCherry) and we used spinning disk confocal videomicroscopy to record the dynamics of BDNF-mCherry containing vesicles within microchannels in the axons (Fig. 1A and Movie EV1). The dynamics of vesicles are in agreement with our recent studies using this technology (Virlogeux *et al*, 2018; Moutaux *et al*, 2018).

We transfected neurons with *Mecp2* siRNA, which reduced Mecp2 protein levels by 63% compared to WT (Fig. EV1A). This reduced the mean velocity and overall linear flow of BDNF vesicles reaching the corticostriatal contacts (Fig. 1B). The number of moving vesicles was unchanged (Fig. EV1B).

HTT phosphorylation status influences anterograde and retrograde BDNF transport

Overexpression of phosphorylated HTT at S421 leads to increased outward transport in cells (Colin *et al*, 2008), but the role of endogenous HTT phosphorylation in axons remains unknown. We isolated cortical neurons from homozygous knock-in mice in which S421 of HTT was replaced by an alanine (*HTT*$^{S421A/S421A}$ or HTT_{SA}), mimicking the absence of phosphorylation, or by an aspartic acid (*HTT*$^{S421D/S421D}$ or HTT_{SD}), mimicking constitutive phosphorylation (Thion *et al*,

2015). Mutating HTT at S421 abrogated the capacity of our phospho-HTT specific antibody to recognize endogenous phosphorylated protein (Fig. EV1C). Importantly, the S into A or into D mutations had no effect on HTT protein levels, as quantification showed no difference in HTT protein expression between WT, HTT_{SD}, and HTT_{SA} mice (Fig. EV1C). Also, we found that the mutations had no effect on cell viability, as shown by the MTT assay (Fig. 1C). We then reproduced a corticostriatal network by plating the neurons within microfluidic devices. Phospho-mimetic HTT (HTT_{SD}) significantly increased the speed of BDNF vesicles moving in the anterograde direction (Fig. 1D, Movie EV1) without affecting the number of moving BDNF vesicles (Fig. EV1D). In contrast, the absence of HTT phosphorylation (HTT_{SA}) significantly increased the retrograde velocity of BDNF vesicles (Fig. 1D). Thus, HTT phosphorylation status influences the velocity of BDNF vesicles in axons.

We next investigated whether HTT phosphorylation status influences the observed dysregulation of BDNF transport in *Mecp2* siRNA-transfected neurons (Fig. 1E and Fig. EV1E and F). Phospho-mimetic HTT (HTT_{SD}) rescued both anterograde and retrograde transport of BDNF, along with the mean velocity of BDNF vesicles and linear flow (Fig. 1E). Preventing HTT phosphorylation (HTT_{SA}) restored only the retrograde velocity of BDNF and linear flow rate to control levels (Fig. 1E). The overall effect of HTT phosphorylation on BDNF transport under normal or low-Mecp2 conditions was not due to a change in the number of moving BDNF vesicles (Fig. EV1D and F) or in cell viability, since we observed no toxicity in *Mecp2* siRNA-transfected HTT_{SD} or HTT_{SA} neurons compared to *Mecp2* siRNA-transfected WT neurons (Fig. 1F). These results demonstrate that genetically promoting HTT phosphorylation at S421 rescues the transport of BDNF vesicles in projecting corticostriatal siMecp2 neurons.

Constitutive phosphorylation of HTT rescues corticostriatal BDNF transport and increases postsynaptic TrkB phosphorylation and markers of postsynaptic density *in vivo*.

Mecp2 KO mice show altered corticostriatal connections and reduced BDNF levels in the striatum (Roux *et al*, 2012). We therefore assessed the impact of huntingtin phosphorylation on BDNF transport *in vivo*. We crossed *Mecp2* KO mice with either HTT_{SA} or HTT_{SD} mice. The resulting double mutant male mice, deficient for the *Mecp2* gene (KO) and homozygous for the S421A ($HTT^{S421A/S421A}$) or S421D mutation ($HTT^{S421D/S421D}$), will from hereon be referred to as KO/HTT_{SA} and KO/HTT_{SD}, respectively. Most of the BDNF protein located in the striatum comes

from the cortex by anterograde transport within corticostriatal afferences (Altar *et al*, 1997). We therefore quantified the level of BDNF proteins using ELISA at the site of translation (the cortex) and the target site (the striatum) of 55-day-old WT mice, KO, KO/HTT_{SD} and KO/HTT_{SA} mice (Fig. 2A). The ratio of striatal and cortical BDNF is an indicator of the *in vivo* efficacy of BDNF axonal transport to the corticostriatal synapses. The ratio we observed in KO/HTT_{SD} mice (1.57±0,3) was equivalent to what we observed in WT mice (1,57±0.6), and was significantly higher than that in *Mecp2* KO mice (1.14±0.1) or KO/HTT_{SA} mice (1.1±0.2). These results suggest that HTT phosphorylation rescues corticostriatal BDNF transport *in vivo*.

We also found that improved corticostriatal BDNF transport in KO HTT_{SD} mice increased levels of TrkB phosphorylation at the postsynaptic level compared to KO WT (+ 36%, $p<0.05$) and KO HTT_{SA} (+ 35%, $p<0.05$), showing that the BDNF release is stimulated *in vivo* (Fig. 2A, Fig. EV1G). As a consequence, the postsynaptic marker PSD-95 is increased in KO HTT_{SD} striatum compared to KO WT striatum (+ 37%, $p<0.01$) (Fig. 2A, Fig. EV1G). We conclude that promoting HTT phosphorylation stimulates striatal BDNF pathways and helps maintain corticostriatal synapse homeostasis *in vivo*.

Constitutive phosphorylation of HTT reduces the loss of body weight of *Mecp2* KO mice and extends their lifespan

We next investigated whether manipulating HTT phosphorylation *in vivo* could have an effect *on Mecp2* KO mouse symptoms. We first assessed the behavior of HTT_{SA} and HTT_{SD} homozygous mice using a modified SHIRPA primary screen (Appendix Table S1) and various behavioral assays (Fig. EV2, A-D) and found no significant differences between WT and HTT_{SA} or HTT_{SD} mice at six months in motor activity, strength, coordination, exploratory behavior, or body weight. *Mecp2* KO mice carrying the S421D mutation (KO/HTT_{SD}) had a longer lifespan than *Mecp2* KO mice, though they still were subject to premature lethality, whereas KO/HTT_{SA} mice showed no improvement over that of *Mecp2* KO mice (Fig. 2B). KO/HTT_{SD} mice also had greater body weight than the *Mecp2* KO mice, whereas the absence of phosphorylation in the KO/HTT_{SA} mice had no effect on weight (Fig. 2C and Fig. EV2E).

Constitutive phosphorylation of HTT reduces apneas in *Mecp2* KO mice

Breathing disturbances are prominent and deleterious in RTT patients (Kerr *et al*, 1997) and

Mecp2 KO mice (Viemari *et al*, 2005). We found that apnea frequency increased with age in *Mecp2* KO mice, from P35 to P55 (Fig. 2D). The KO/HTT_{SD} mice had significantly fewer apneas than *Mecp2* KO mice at both time points (Fig. 2D). The absence of HTT phosphorylation slightly worsened this phenotype.

These data suggest that promoting HTT phosphorylation *in vivo* improves respiration in *Mecp2* KO mice.

Constitutive phosphorylation of HTT improves motor function of *Mecp2* KO mice

We next investigated motor coordination on the accelerating rotarod test (Pratte *et al*, 2011). In agreement with previous studies, *Mecp2* KO mice showed a progressive, significant decrease in the latency to fall relative to WT mice (Fig. 2E). Promoting HTT phosphorylation delayed the appearance of motor incoordination until P55, but ablating HTT phosphorylation worsened motor coordination at both time points (Fig. 2E). HTT phosphorylation had no effect on the overall exploration pattern of *Mecp2* KO mice in the open-field (OF) test (Fig. EV2F), but the time before initiation of the first movement was significantly longer for the *Mecp2* KO than WT mice (Fig. 2F). The latency to explore the OF arena was further increased in KO/HTT_{SA} mice, whereas it was reduced in the KO/HTT_{SD} mice towards the values observed for WT mice (Fig. 2F).

We next monitored circadian activity and found no deregulation in the circadian rhythm in the different genotypes during the day (Fig. EV2G). There was, however, a striking suppression of spontaneous locomotion in the absence of *Mecp2* during the dark phase (7:00 PM - 7:00 AM) (Fig. EV2G). Promoting HTT phosphorylation enhanced spontaneous night activity, increasing the distance travelled by the KO/HTT_{SD} mice, although it did not reach the value of the WT mice (Fig. EV2H). Conversely, the distance travelled by the KO/HTT_{SA} mice was significantly less than that covered by the KO/HTT_{SD} mice. Overall, these results show that promoting HTT phosphorylation improves sensorimotor coordination and locomotor activity in *Mecp2* KO mice.

Inhibition of calcineurin by FK506 restores BDNF transport in Mecp2-silenced axons

Since chronic phosphorylation rescues BDNF trafficking *in vitro* and improves symptoms in mice, we investigated whether pharmacological induction of HTT phosphorylation could be of therapeutic value in RTT. We previously reported that HTT phosphorylation can be inhibited by the protein phosphatase calcineurin (Pardo *et al*, 2006; Pineda *et al*, 2009). We therefore evaluated

whether FK506, a calcineurin inhibitor, can restore BDNF transport in *Mecp2*-silenced neurons by increasing HTT phosphorylation. Cortical neurons connected to striatal neurons within the microfluidic devices were transduced with the BDNF-mCherry lentiviral vector and a siRNA targeting either a control sequence or that of *Mecp2*. Five days after plating, we incubated the microfluidic chambers for 1 h with 1 µM FK506 or vehicle and recorded BDNF axonal transport.

FK506 treatment increased HTT phosphorylation (Fig. 3A) and rescued the reduced BDNF trafficking measured after Mecp2 silencing (Fig. 3B and C, Movie EV2). Both mean anterograde and retrograde vesicle velocities were increased in si*Mecp2*-transfected neurons, with a significant overall effect on mean velocity and linear flow (Fig. 3C). The number of moving vesicles did not change (Fig. 3C). FK506-induced calcineurin inhibition thus mitigates deficits of BDNF transport observed in Mecp2-silenced neurons.

FK506 increases HTT phosphorylation in *Mecp2* KO mice

To determine whether calcineurin inhibition via FK506 treatment could improve *Mecp2* KO mouse symptoms, we treated *Mecp2* KO, WT and WT HTT_{SA} mice with FK506 to induce HTT phosphorylation. Mice were first injected intraperitoneally with FK506 (5 mg/kg) and sacrificed 2 h after administration, as previously described (Pardo *et al*, 2006). We analyzed HTT phosphorylation at S421 by immunoblotting fresh whole-brain protein extract (Fig. 4A and Fig. EV3A and B). As previously described, administration of FK506 in WT mice increased HTT phosphorylation, by about 1.3-fold (Pardo *et al*, 2006). In *Mecp2* KO mice, FK506 doubled HTT phosphorylation relative to vehicle. FK506 had no effect on HTT phosphorylation in WT HTT_{SA} mice (Fig. EV3A and B)

FK506 treatment improves respiration and motor function of *Mecp2* KO mice and extends their lifespan via HTT phosphorylation

To determine whether FK506 could improve the Mecp2-deficient phenotype, we treated *Mecp2* KO mice by intraperitoneal FK506 injection (10 mg/kg), three times a week, starting at P30. We choose P30 as a starting point, since the onset of the Mecp2-knockout phenotype is already apparent at this stage as breathing abnormalities, locomotor deficits and body weight loss (Guy *et al*, 2001; Viemari *et al*, 2005; Matagne *et al*, 2017). FK506 treatment significantly increased the lifespan of *Mecp2* KO mice (Fig. 4B) and induced a significant increase in body

weight by P55 (Fig. 4C). The number of apneas was significantly lower in the FK506-treated group than the vehicle group at P35 and remained lower at P55 (Fig. 4D). FK506-treated *Mecp2* KO mice performed better on the accelerating rotarod at P50 (Fig. 4E) and showed better forelimb muscle strength than the vehicle group (Fig. 4F). We next investigated cell death in the striatum of these mice. In accord with previous reports (Reiss *et al*, 1993; Kishi & Macklis, 2004; Armstrong, 2005; Roux *et al*, 2007), we did not detect any cell death in Mecp2 mice by cleaved-Caspase 3 immunodetection or by TUNEL assay (Fig. EV4A and B). Importantly, we found that FK506 treatment did not induce any neuronal toxicity or cell death after 20 days of treatment (Fig. EV4A and B).

We also verified the induction of HTT phosphorylation in Mecp2-deficient mice after 20 days of FK506 chronic treatment. Mouse brain samples were analyzed 2 hrs after the last treatment. We did not detect any difference in Mecp2 protein levels or in HTT phosphorylation in wild-type mice treated with FK506 (Fig. EV3B and C). However, at this time point we did not detect elevated HTT phosphorylation in the samples treated with FK506 relative to DMSO-treated animals, likely because repeated treatments desensitize the pathway. We observed a trend toward reduction in cFos staining in Mecp2-deficient mice that was increased back to control levels in FK506-treated *Mecp2* KO mice, suggesting a positive treatment effect (Fig. EV4C and D).

To establish that the beneficial effect of FK506 is mediated by HTT phosphorylation at S421, we treated KO HTT_{SA} mice by intraperitoneal FK506 injection as previously done (Fig. 4). Interestingly, the lifespan of *Mecp2* KO/HTT_{SA} mice was significantly shorter than that of *Mecp2* KO mice (Fig. 4B). Moreover, FK506 treatment affected neither motor function nor apneas of KO HTT_{SA} mice (Fig. 4D, E and F). These results demonstrate that HTT phosphorylation at S421 is essential for the therapeutic effect of FK506.

Discussion

Here, we demonstrate that genetically or pharmacologically inducing HTT phosphorylation at S421 rescues BDNF vesicular transport in Mecp2-silenced projecting corticostriatal neurons and improves several pathophysiological features of *Mecp2* KO mice. The ability of FK506 as a proof-of-principle candidate to improve Mecp2 symptoms highlights the feasibility of pharmacological stimulation of HTT S421-P in a mouse model of RTT. Importantly, our findings show that HTT phosphorylation can stimulate endogenous machinery to promote BDNF

trafficking in the corticostriatal network.

There has been considerable interest in modulating BDNF expression and signaling as a treatment for RTT. Unfortunately, BDNF itself has very low blood-brain-barrier (BBB) permeability, precluding its peripheral administration as a potential therapy. Several studies have used indirect stimulation of BDNF metabolism via fingolimod (Deogracias *et al*, 2012) or ampakine treatment (Ogier *et al*, 2007) to circumvent this limitation, but these pharmacological treatments only partially improved the phenotype of *Mecp2* KO mice. Daily injection of IGF1, another neurotrophic factor that can cross the BBB and is known to induce Akt phosphorylation (Humbert *et al*, 2002), has been found to improve survival, locomotor activity and respiratory rhythm in *Mecp2* KO mice (Tropea *et al*, 2009). Finally, potential agonists of the TrkB receptor, such as 7,8-dihydroxyflavone (Johnson *et al*, 2012) and LM22A-4 (Schmid *et al*, 2012; Kron *et al*, 2014; Li *et al*, 2017), improved breathing patterns in *Mecp2* KO mice. It is important to note, however, that the improvements observed in these different studies required that pharmacological treatments be initiated before the appearance of the first symptoms.

Given that RTT is not diagnosed until long after symptoms have begun, we searched for a more practical translational approach based on observed improvements in the RTT phenotype by constitutive phosphorylation of HTT. We selected FK506 because Pardo *et al.* (Pardo *et al*, 2006) found that this drug increases phosphorylation of mutant HTT. Importantly, FK506 also induces HTT phosphorylation in *Mecp2* KO mice. Our results showed that FK506 treatment, starting at an already-symptomatic stage, improved the lifespan, motor strength and coordination, exploratory behavior, and reduced the frequency of apneas in *Mecp2* KO mice in a manner that requires HTT phosphorylation at S421. Thus, part of the beneficial effect of FK506 treatment is due to the stimulation of the HTT-dependent transport of BDNF. It is possible that FK506 also modulates the trafficking of other cargo, such as mitochondria, which could contribute to the *in vivo* improvement we saw in the *Mecp2* KO mice. Future studies investigating such additional effects would be of interest, as they would increase the therapeutic relevance of FK506 treatment for Mecp2 symptoms (Reddy *et al*, 2012).

We conclude that BDNF trafficking and supply are diminished in the absence of Mecp2 and can be effectively stimulated by promoting HTT phosphorylation. Our results are in accord with a recent study that demonstrated that BDNF acts cell-autonomously in an autocrine loop, as wild-type neurons were unable to rescue growth deficits of neighboring *Mecp2*-deficient neurons

(Sampathkumar *et al*, 2016). Thus, HTT phosphorylation may increase the bioavailability of BDNF at the synapse through autocrine and paracrine mechanisms in the brains of *Mecp2 KO* mice and likely represents a strategy of therapeutic interest versus a general, non-synapse-specific increase of BDNF levels in the brain.

Materials and Methods

Mouse breeding and genotyping

All mouse lines were on a C57BL/6J genetic background. The Mecp2tm1-1Bird Mecp2-deficient mice were obtained from the Jackson Laboratory and maintained on a C57BL/6 background by using C56BL/6J male breeders (also from the Jackson Laboratory). The HTT knock-in mice were previously generated by inserting a point mutation in exon 9 (AGC>GAC, Ser>Asp called S421D or AGC>GCC, Ser>Ala called S421A) (Thion *et al*, 2015). To obtain double mutant mice (*Mecp2* KO and S421A or S421D), heterozygous females ($Mecp2^{+/-}$) were crossed with homozygous S421D or S421A males.

Hemizygous mutant males ($Mecp2^{-/y}$ also called *Mecp2* KO) were generated by crossing heterozygous females ($Mecp2^{+/-}$) with C57BL/6 males. Genotyping was performed by routine PCR technique following a previously described protocol (Roux *et al*, 2012). Animals were housed under standard conditions of temperature (21 ± 2°C) and humidity (55 ± 5%), with food and water ad libitum in a 12:12h day/night cycle.

Experimental protocols were approved by the ethical committee of the Aix Marseille University and the French M.E.N.E.S.R. minister (Permit Number: 02910.02).

The experimental procedures were carried out in keeping with the European guidelines for the care and use of laboratory animals (EU directive 2010/63/EU), the guide for the care and use of the laboratory animals of the French national institute for science and health (INSERM). All experiments were made to minimize animal suffering. In order to reduce animal suffering, endpoints were fixed as weight loss limit (below 80% of maximum weight), obvious breathing defects or severe injury. In these cases, animals were euthanized with an overdose of pentobarbital (100mg/kg BW i.p., Ceva Santé Animale, La Ballastiere, France).

FK506 chronic *in vivo* treatment of Mecp2-deficient mice (KO and KO HTT_{SA})

Mecp2 KO mice were randomly assigned in groups. From P30, animals received an i.p. injection three times a week of either 10mg/kg FK506 in 17% DMSO or vehicle alone (17% DMSO). The first group was used for behavioral testing and evaluating survival (see below). A second group was used to assess the chronic effects of FK506 treatment from P30 to P50 on cellular and molecular parameters.

Behavioral testing

All mice were weighed every five days and assessed for survival. At P35, P45 and P55, each animal underwent a set of behavioral tests to assess motor function, activity and breathing pattern (Figure 2). All testing occurred during the light phase of the light-dark cycle (except for the PhenoRack monitoring). All the behavioral experiments were performed blinded to HTT genotype and treatment.

Open Field: an arena made of clear perspex (38x30 cm), under controlled light conditions (300lx), was used for the FK506 study. For the genetic study, mice were placed in a 1 meter diameter arena under controlled light conditions (300lx). Activity was recorded using the Videotrack software (Viewpoint, Lyon, France) for 20 minutes. Activity and average velocity (cm/s) were determined from the total distance moved and activity duration. Vertical activity (rearing, leaning and grooming) was noted by an experimenter blind of the genotype.

Rotarod: sensorimotor abilities were assessed by the accelerating Rotarod apparatus (Panlab LE-8200, Harvard Apparatus). Each trial started at 4rpm and reached 40rpm speed after 300s. Mice underwent 3 trials, with 5 min rest time in between. The trial ended when the mouse fell off the rod or after 300 s. Latency to fall (in second) was measured and only the best trial was recorded. In the case of mice clinging to the rod, the trial was stopped and the passive rotation was considered a failure in performance like falling (Brown *et al*, 2005) .

Grip strength: A Bioseb grip strength meter (Panlab) was used to measure forelimb strength. Five measures for each mouse was taken and means were calculated from the three best trials.

Whole body plethysmography: To assess apneas, mice were placed in a clear plexiglass chamber (200ml) and allowed to breathe naturally under conscious and unrestrained conditions. After a ~30 min adaptation, breathing was recorded: the spirogram was obtained by recording the pressure difference between the two chambers, then the signal was amplified, filtered and fed to an analog-to-digital converter (sampling frequency, 1 kHz) and finally analyzed by the Spike2 interface and software (v.5.04, Cambridge Electronic Design Ltd., Cambridge, UK). Apneas were defined by more than 1s without breathing, as previously described (Roux *et al*, 2007). Breathing cycles were divided into four groups according to their duration: hyperventilation (including cycles in the range 0–0.3 s range); ventilation (0.3–0.7 s); hypoventilation (0.7–1 s) and apneas (1– ∞ s). The breathing variability was calculated as the mean standard variability. Breathing parameters were

obtained from the analysis of quiet period of at least 100 consecutive cycles (Fig. EV5).

Home cage activity: To analyze spontaneous activity and circadian rhythm, mice were put in individual cages and monitored by the PhenoRack system (Viewpoint, Lyon, France). Mice locomotion was tracked by infrared light during 48h, after a 24h adaptation phase only the last 24h activity was analyzed. The recorded data allowed us to analyze activity, distance (cm) and velocity (cm/sec).

BDNF Immunoassay:

P55 (n=4 Wt; n=4 Mecp2 KO; n=4 KO HTT_{SD}; n=5 KO HTT_{SA}) male mice were euthanized by cervical dislocation, and their brains were dissected out within the first two minutes post-mortem. The cortex and the striatum were microdissected using a punching needle (0.5 mm in diameter). Briefly, brain area dissection was performed on cryostat brain sections with the help of a 5X magnifying lens, following their stereotaxic coordinates (Paxinos and Franklin, 2001). We dissected cortical and striatal samples only coming from the same slice in the same rostro-caudal level. Tissue samples were freshly isolated and lysed in 200 µ l of the extraction buffer (100 mM Tris-pH7.5, 125 mM NaCl, 0.1 mM EGTA, 0.1% TritonX-100, Roche® protease inhibitors cocktail), sonicated, centrifugated. The supernatant was stored at − 80 °C until assay. Total protein concentration was determined by using the bicinchoninic acid (BCA) protein assay (Thermofisher scientific) and measured with a spectrophotometer (Glomax, Promega). The level of BDNF protein from tissue extracts was determined with the BDNF Emax® ImmunoAssay System (Promega) using the manusfacturer's instruction. In the present study we measured only free mature BDNF, therefore we proceeded directly to the ELISA protocol avoiding any acid treatment. In each assay, duplicate wells were assigned for each sample. A Victor 4 Perkin Elmer microplate reader was used to measure signal intensity from the wells at 450 nm. A linear standard curve was generated with standard BDNF from 5.8 to 500 pg/ml. The total amount of BDNF per well was calculated based on the standard curve and each sample value was within the linear range. The Relative BDNF value was then calculated by normalizing the amount of BDNF against the total amount of protein input.

Western Blotting

Adult (P55) male mice were euthanized by cervical dislocation, and their brains were

dissected out within the first 2 min post-mortem. Brains were dissected on ice and proteins were extracted by sonication and isolated in a lysis buffer containing 50mM Tris–HCl (ph = 7.5), 150 mM NaCl, 2 mM EGTA, 2mM EDTA, 1% Triton X-100, 10nM betaglycerophosphate, 5mM Sodium pyrophosphate, 50mM sodium fluoride and Halt™ proteases and phosphatases inhibitor cocktail (Pierce Thermofisher). Proteins were extracted from neuronal culture with lysis buffer containing 4 mM Hepes, pH 7.4, 320 mM sucrose and protease inhibitor cocktail (Roche). Protein concentrations were determined by the bicinchoninic acid method. After a denaturation step at 96 °C for 5 min, proteins (100 µg) were separated on 4-20% SDS-polyacrylamide gel (Life technology) and transferred onto a nitrocellulose membrane by electroblotting using the Trans-Blot turbo transfer system (Bio-Rad). The membrane was blocked with blocking buffer (Millipore, WBAVDFL01) for 1 h at room temperature. Primary antibodies for HTT (1:1000, rabbit, clone D7F7, CST(Lunkes *et al*, 2002)), HTT-pS421 (1:500. rabbit homemade previously described (Humbert *et al*, 2002)), Mecp2 (1:1000, rabbit, CST), TRKB-p816 (Millipore ABN1381), PSD-95 (1:1000, Neuromab), Tubulin (1:5000, mouse, Sigma) GAPDH (1:5000, rabbit, Sigma), Actin (1:10000, mouse, Millipore), Calnexin (1:1000, rabbit, Sigma C4731) were diluted in the same solution and incubated overnight at 4 °C. The membrane was incubated using appropriate HRP secondary antibodies (donkey anti-rabbit 711-035-152, donkey anti-mouse 715-035-150, Jackson Immunoresearch Laboratory and Biorad ChemiDoc XRS System) or fluorescent secondary antibodies (IRDye 800 CW, IRDye 680 RD, LI-COR and LI-COR odyssey Imager). Quantitative analyses of signal intensity were performed using ImageJ software. For quantification, total (phosphoindependent) protein signals were used to normalize the phospho-protein signal.

Immunohistochemistry

Mice were euthanized with pentobarbital and transcardially perfused with 0.01M PBS followed by 4% paraformaldehyde (PFA) in phosphate buffer. Brains were removed, fixed in 4% PFA overnight at 4°C, and then cryopreserved in 20% sucrose for three days. Brains were then rapidly frozen, and coronally sectioned into 50 µm sections using a Leica VT1200s cryostat (Leica Biosystems). Sections were rehydrated in PBS 3 times for 10 minutes and blocked with 7% normal goat serum in PBS for 1 hour and then incubated overnight at room temperature (RT) with anti-cFos (1/200, rabbit, Abcam ab209794) or anti-Cleaved-Caspase 3 (1/400, rabbit, Cell signaling) antibodies. The sections were then washed three times for 10 minutes each in PBS followed by

incubation for 2 hours with the following secondary antibodies: Alexa Fluor 488-labeled goat anti-rabbit at 1/400. After staining, the sections were washed three times, for 10 minutes each in PBS and then incubated 10 minutes in DAPI. After a last 10-minute wash, sections were mounted in Immu-mount (Thermo Scientific). The immunolabeled slices were digitized and recorded using an Apotome Axioimager 2 (Carl Zeiss) or a Zeiss Lumar stereomicroscope coupled to Axiocam digital camera (Axiovision 4.4, Carl Zeiss).

Videomicroscopy

Embryonic (E15.5) neuronal cultures were prepared as previously described (Liot *et al*, 2013). Ganglionic eminences and cortex were dissected and dissociated cortical neurons were nucleofected with ON-TARGET plus mouse Mecp2 siRNA or Non-targeting siRNA 1 (Dharmacon) according to the protocol of Amaxa Nucleofection (Lonza). Then neurons were plated into microchambers coated with poly-D-lysine (0.1 mg/ml) in the cortical and synaptic compartment or poly-D-lysine and laminin (10 µg/ml, Sigma) into the striatal compartment and cultured at 37°C in a 5% CO2 incubator for 5 days. After 24h in culture, cortical neurons were transduced with lentivector coding for BDNF-mCherry into presynaptic neuron chamber for axonal transport analysis as previously described (Virlogeux *et al*, 2018). Acquisitions were done on microgrooves, at the limit of the synaptic compartment, at 5 Hz for 30 seconds on inverted microscope (Axio Observer, Zeiss) coupled to a spinning-disk confocal system (CSU-W1-T3; Yokogawa) connected to an electron-multiplying CCD (charge-coupled device) camera (ProEM+1024, Princeton Instrument) at 37 °C and 5% CO2. Quantifications of vesicle velocity, linear flow rate and vesicle number was done on 100 µm of axon using KymoTool Box ImageJ plugin as previously described (Zala *et al*, 2013; Virlogeux *et al*, 2018). Vesicle velocity corresponds to segmental anterograde or retrograde velocity. Directional net flux is the anterograde cumulative distance minus the retrograde cumulative distance. Regarding vesicle number, a vesicle is considered anterograde when the distance travelled by one vesicle is more anterograde than retrograde.

MTT Assay

In a corticostriatal network, at DIV 11 or 12, presynaptic chamber was filled with MTT $1/10^{e}$ from MTT solution at 5 mg/mL. After a 3,5-hours incubation at 37°C, MTT solution was carefully

removed from the presynaptic chamber and MTT solvent was added (10% SDS, 1,2mM HCl) for 30 minutes under agitation. Then, MTT solvent was removed from the microfluidics device and put in a well within a 96 well pate. The absorbance was read at 490 nm on a microplate reader (PHERAstar FS, BMG labtech). Negative controls (dead cells) were treated with H_2O_2 at 100mM for 48h before the experiment.

Terminal deoxynucleotidyl transferase dUTP nick end labeling (TUNEL) of apoptotic cells

Cell apoptosis was measured in vivo using the Click-It™ Plus TUNEL Assay (Invitrogen) according to the manufacturer's protocol.

Statistical analysis

All analyses were performed using GraphPad Prism for Windows/MacOS (GraphPad Software, La Jolla, California, USA, www.graphpad.com). The results are reported as mean +/- standard error of the mean (S.E.M). A p-value < 0.05 was considered to be statistically significant. For group comparisons normality distribution of the datasets were tested before performing any statistical test by Shapiro's test. In case of non normal distribution, a non parametric test was perfomed. When ANOVA was used, Brown Forsythe's test verifies that the variance is homogenous. One-way ANOVAs were performed as indicated with Dunnett's post-hoc analysis for pairwise comparisons when normal distribution. Kruskal-Wallis test with Dunn's multiple comparison were performed on datasets without normal distribution. When appropriate, two groups were compared with an unpaired two-way t test or Mann-Whitney test on datasets without normal distribution. The Kaplan–Meier log-rank test was used for survival studies.

Acknowledgements

We thank S. Humbert for sharing the *HTT*^{S421A} and *HTT*^{S421D} mice and for advice; the GIN imaging facility (PIC-GIN) for help with image acquisitions; G. Froment, D. Nègre, and C. Costa from the lentivirus production facility of SFR Biosciences (UMS3444/CNRS, US8/Inserm, ENS de Lyon, UCBL); and V. Brandt for critical reading of the manuscript. This work was supported by grants from Agence Nationale pour la Recherche (ANR-2012-BSV1-0003-03 ANTARES, J.C.R. & F.S., ANR-14-CE35-0027-01 PASSAGE, F.S.; ANR-15-JPWG-0003-05 EU Joint Program-Neurodegenerative Disease (JPND) Research project CircProt (no. 643417), (F.S.), Fondation pour la Recherche Médicale (FRM, équipe labellisée, F.S.), Fondation Bettencourt Schueller (F.S.), Fédération pour la Recherche sur le Cerveau (F.S.), Inserm (J.C.R. & F.S.), Aix-Marseille Université (J.C.R.), AFSR (J.C.R.) and NeuroCoG in the framework of the "Investissements d'avenir" program (ANR-15-IDEX-02, F.S.). F.S. laboratory is member of the Grenoble Center of Excellence in Neurodegeneration (GREEN).

Author contributions

YE, JB, NP, YSA, BD, LV, FS and JCR designed experiments. YE, JB, NP, YSA, LS, VM, CS, EB and HV performed experiments. YE, JB, NP, YSA, LS, VM, CS, HV, BD, LV, FS, EB and JCR analyzed the data and YE, JB, FS and JCR wrote the manuscript.

Conflict of interest

The authors declare that they have no conflict of interest.

Bibliography

Altar CA, Cai N, Bliven T, Juhasz M, Conner JM, Acheson AL, Lindsay RM & Wiegand SJ (1997) Anterograde transport of brain-derived neurotrophic factor and its role in the brain. *Nature* **389:** 856–860

Amir RE, Van den Veyver IB, Wan M, Tran CQ, Francke U & Zoghbi HY (1999) Rett syndrome is caused by mutations in X-linked MECP2, encoding methyl-CpG-binding protein 2. *Nat. Genet.* **23:** 185–188

Armstrong DD (2005) Neuropathology of Rett syndrome. *J. Child Neurol.* **20:** 747–753

Brown SDM, Chambon P, de Angelis MH & Eumorphia Consortium (2005) EMPReSS: standardized phenotype screens for functional annotation of the mouse genome. *Nat. Genet.* **37:** 1155

Chahrour M, Jung SY, Shaw C, Zhou X, Wong STC, Qin J & Zoghbi HY (2008) MeCP2, a key contributor to neurological disease, activates and represses transcription. *Science* **320:** 1224–1229

Chang Q, Khare G, Dani V, Nelson S & Jaenisch R (2006) The disease progression of Mecp2 mutant mice is affected by the level of BDNF expression. *Neuron* **49:** 341–348

Chen L, Chen K, Lavery LA, Baker SA, Shaw CA, Li W & Zoghbi HY (2015) MeCP2 binds to non-CG methylated DNA as neurons mature, influencing transcription and the timing of onset for Rett syndrome. *Proc. Natl. Acad. Sci. USA* **112:** 5509–5514

Chen WG, Chang Q, Lin Y, Meissner A, West AE, Griffith EC, Jaenisch R & Greenberg ME (2003) Derepression of BDNF transcription involves calcium-dependent phosphorylation of MeCP2. *Science* **302:** 885–889

Cheng P-L, Song A-H, Wong Y-H, Wang S, Zhang X & Poo M-M (2011) Self-amplifying autocrine actions of BDNF in axon development. *Proc. Natl. Acad. Sci. USA* **108:** 18430–18435

Cheng T-L, Wang Z, Liao Q, Zhu Y, Zhou W-H, Xu W & Qiu Z (2014) MeCP2 suppresses nuclear microRNA processing and dendritic growth by regulating the DGCR8/Drosha complex. *Dev. Cell* **28:** 547–560

Colin E, Zala D, Liot G, Rangone H, Borrell-Pagès M, Li X-J, Saudou F & Humbert S (2008) Huntingtin phosphorylation acts as a molecular switch for anterograde/retrograde transport in neurons. *EMBO J.* **27:** 2124–2134

Deogracias R, Yazdani M, Dekkers MPJ, Guy J, Ionescu MCS, Vogt KE & Barde Y-A (2012) Fingolimod, a sphingosine-1 phosphate receptor modulator, increases BDNF levels and improves symptoms of a mouse model of Rett syndrome. *Proc. Natl. Acad. Sci. USA* **109:** 14230–14235

Guy J, Hendrich B, Holmes M, Martin JE & Bird A (2001) A mouse Mecp2-null mutation causes neurological symptoms that mimic Rett syndrome. *Nat. Genet.* **27:** 322–326

Humbert S, Bryson EA, Cordelières FP, Connors NC, Datta SR, Finkbeiner S, Greenberg ME & Saudou F (2002) The IGF-1/Akt pathway is neuroprotective in Huntington's disease and involves Huntingtin phosphorylation by Akt. *Dev. Cell* **2:** 831–837

Johnson RA, Lam M, Punzo AM, Li H, Lin BR, Ye K, Mitchell GS & Chang Q (2012) 7,8-dihydroxyflavone exhibits therapeutic efficacy in a mouse model of Rett syndrome. *J. Appl. Physiol.* **112:** 704–710

Katz DM, Bird A, Coenraads M, Gray SJ, Menon DU, Philpot BD & Tarquinio DC (2016) Rett syndrome: crossing the threshold to clinical translation. *Trends Neurosci.* **39:** 100–113

Kerr AM, Armstrong DD, Prescott RJ, Doyle D & Kearney DL (1997) Rett syndrome: analysis of deaths in the British survey. *Eur. Child Adolesc. Psychiatry* **6 Suppl 1:** 71–74

Kishi N & Macklis JD (2004) MECP2 is progressively expressed in post-migratory neurons and is involved in neuronal maturation rather than cell fate decisions. *Mol. Cell. Neurosci.* **27:** 306–321

Kron M, Lang M, Adams IT, Sceniak M, Longo F & Katz DM (2014) A BDNF loop-domain mimetic acutely reverses spontaneous apneas and respiratory abnormalities during behavioral arousal in a mouse model of Rett syndrome. *Dis. Model. Mech.* **7:** 1047–1055

Li W, Bellot-Saez A, Phillips ML, Yang T, Longo FM & Pozzo-Miller L (2017) A small-molecule TrkB ligand restores hippocampal synaptic plasticity and object location memory in Rett syndrome mice. *Dis. Model. Mech.* **10:** 837–845

Liot G, Zala D, Pla P, Mottet G, Piel M & Saudou F (2013) Mutant Huntingtin alters retrograde transport of TrkB receptors in striatal dendrites. *J. Neurosci.* **33:** 6298–6309

Lunkes A, Lindenberg KS, Ben-Haïem L, Weber C, Devys D, Landwehrmeyer GB, Mandel J-L & Trottier Y (2002) Proteases acting on mutant huntingtin generate cleaved products that differentially build up cytoplasmic and nuclear inclusions. *Mol. Cell* **10:** 259–269

Lyst MJ & Bird A (2015) Rett syndrome: a complex disorder with simple roots. *Nat. Rev. Genet.* **16:** 261–275

Matagne V, Ehinger Y, Saidi L, Borges-Correia A, Barkats M, Bartoli M, Villard L & Roux J-C (2017) A codon-optimized Mecp2 transgene corrects breathing deficits and improves survival in a mouse model of Rett syndrome. *Neurobiol. Dis.* **99:** 1–11

Meehan RR, Lewis JD & Bird AP (1992) Characterization of MeCP2, a vertebrate DNA binding protein with affinity for methylated DNA. *Nucleic Acids Res.* **20:** 5085–5092

Moutaux E, Christaller W, Scaramuzzino C, Genoux A, Charlot B, Cazorla M & Saudou F (2018) Neuronal network maturation differently affects secretory vesicles and mitochondria transport in axons. *Sci. Rep.* **8:** 13429

Ogier M, Wang H, Hong E, Wang Q, Greenberg ME & Katz DM (2007) Brain-derived neurotrophic factor expression and respiratory function improve after ampakine treatment in a mouse model of Rett syndrome. *J. Neurosci.* **27:** 10912–10917

Pardo R, Colin E, Régulier E, Aebischer P, Déglon N, Humbert S & Saudou F (2006) Inhibition of calcineurin by FK506 protects against polyglutamine-huntingtin toxicity through an increase of huntingtin phosphorylation at S421. *J. Neurosci.* **26:** 1635–1645

Pineda JR, Pardo R, Zala D, Yu H, Humbert S & Saudou F (2009) Genetic and pharmacological inhibition of calcineurin corrects the BDNF transport defect in Huntington's disease. *Mol. Brain* **2:** 33

Pratte M, Panayotis N, Ghata A, Villard L & Roux J-C (2011) Progressive motor and respiratory metabolism deficits in post-weaning Mecp2-null male mice. *Behav. Brain Res.* **216:** 313–320

Reddy PH, Tripathi R, Troung Q, Tirumala K, Reddy TP, Anekonda V, Shirendeb UP, Calkins MJ, Reddy AP, Mao P & Manczak M (2012) Abnormal mitochondrial dynamics and synaptic degeneration as early events in Alzheimer's disease: implications to mitochondria-targeted antioxidant therapeutics. *Biochim. Biophys. Acta* **1822:** 639–649

Reiss AL, Faruque F, Naidu S, Abrams M, Beaty T, Bryan RN & Moser H (1993) Neuroanatomy of Rett syndrome: a volumetric imaging study. *Ann. Neurol.* **34:** 227–234

Roux J-C, Dura E, Moncla A, Mancini J & Villard L (2007) Treatment with desipramine improves breathing and survival in a mouse model for Rett syndrome. *Eur. J. Neurosci.* **25:** 1915–1922

Roux J-C, Zala D, Panayotis N, Borges-Correia A, Saudou F & Villard L (2012) Modification of Mecp2 dosage alters axonal transport through the Huntingtin/Hap1 pathway. *Neurobiol. Dis.* **45:** 786–795

Sampathkumar C, Wu Y-J, Vadhvani M, Trimbuch T, Eickholt B & Rosenmund C (2016) Loss of MeCP2 disrupts cell autonomous and autocrine BDNF signaling in mouse glutamatergic neurons. *Elife* **5:**

Saudou F & Humbert S (2016) The biology of huntingtin. *Neuron* **89:** 910–926

Schmid DA, Yang T, Ogier M, Adams I, Mirakhur Y, Wang Q, Massa SM, Longo FM & Katz DM (2012) A TrkB small molecule partial agonist rescues TrkB phosphorylation deficits and improves respiratory function in a mouse model of Rett syndrome. *J. Neurosci.* **32:** 1803–1810

Skene PJ, Illingworth RS, Webb S, Kerr ARW, James KD, Turner DJ, Andrews R & Bird AP (2010) Neuronal MeCP2 is expressed at near histone-octamer levels and globally alters the chromatin state. *Mol. Cell* **37:** 457–468

Taylor AM, Dieterich DC, Ito HT, Kim SA & Schuman EM (2010) Microfluidic local perfusion chambers for the visualization and manipulation of synapses. *Neuron* **66:** 57–68

Thion MS, McGuire JR, Sousa CM, Fuhrmann L, Fitamant J, Leboucher S, Vacher S, du Montcel ST, Bièche I, Bernet A, Mehlen P, Vincent-Salomon A & Humbert S (2015) Unraveling the role of huntingtin in breast cancer metastasis. *J. Natl. Cancer Inst.* **107:**

Tropea D, Giacometti E, Wilson NR, Beard C, McCurry C, Fu DD, Flannery R, Jaenisch R & Sur M (2009) Partial reversal of Rett Syndrome-like symptoms in MeCP2 mutant mice. *Proc. Natl. Acad. Sci. USA* **106:** 2029–2034

Van Esch H (2012) MECP2 Duplication Syndrome. *Mol. Syndromol.* **2:** 128–136

Viemari J-C, Roux J-C, Tryba AK, Saywell V, Burnet H, Peña F, Zanella S, Bévengut M, Barthelemy-Requin M, Herzing LBK, Moncla A, Mancini J, Ramirez J-M, Villard L & Hilaire G (2005) Mecp2 deficiency disrupts norepinephrine and respiratory systems in mice. *J. Neurosci.* **25:** 11521–11530

Virlogeux A, Moutaux E, Christaller W, Genoux A, Bruyère J, Fino E, Charlot B, Cazorla M & Saudou F (2018) Reconstituting Corticostriatal Network on-a-Chip Reveals the Contribution of the Presynaptic Compartment to Huntington's Disease. *Cell Rep.* **22:** 110–122

Xu X, Kozikowski AP & Pozzo-Miller L (2014) A selective histone deacetylase-6 inhibitor improves BDNF trafficking in hippocampal neurons from Mecp2 knockout mice: implications for Rett syndrome. *Front. Cell Neurosci.* **8:** 68

Young JI, Hong EP, Castle JC, Crespo-Barreto J, Bowman AB, Rose MF, Kang D, Richman R, Johnson JM, Berget S & Zoghbi HY (2005) Regulation of RNA splicing by the methylation-dependent transcriptional repressor methyl-CpG binding protein 2. *Proc. Natl. Acad. Sci. USA* **102:** 17551–17558

Zala D, Hinckelmann M-V, Yu H, Lyra da Cunha MM, Liot G, Cordelières FP, Marco S & Saudou F (2013) Vesicular glycolysis provides on-board energy for fast axonal transport. *Cell* **152:** 479–491

Fig. 1. Huntingtin phosphorylation rescues BDNF transport in Mecp2-deficient axons.

(**A**) Microchamber that allows the isolation of axons within a corticostriatal network and live-cell imaging of axonal BDNF-mCherry transduced into mouse primary cortical neurons.

(**B**) Representative kymographs and quantification of anterograde, retrograde, mean velocity, and linear flow rate of BDNF-mCherry-containing vesicles in cortical neurons transfected with siMecp2 or siControl (siCtl), inducing significant silencing of Mecp2 (n=3; unpaired t-test).

(**C**) Cell viability in WT, HTT_{SA}, or HTT_{SD} neurons measured by MTT assay. No differences were observed between the different groups (n=3; one-way ANOVA Kruskal-Wallis test, p=0.5701)

(**D**) Quantification of anterograde, retrograde, mean velocity, and linear flow rate of BDNF-mCherry trafficking into cortical neurons obtained from WT, HTT_{SA}, or HTT_{SD} homozygous knock-in mice in which S421 of HTT was replaced by an alanine ($HTT^{S421A/S421A}$ or HTT_{SA}), mimicking the absence of phosphorylation, or by an aspartic acid ($HTT^{S421D/S421D}$ or HTT_{SD}), mimicking constitutive phosphorylation (n = 3; one-way ANOVA test with Tukey's multiple comparisons).

(**E**) Kymographs and quantification of anterograde, retrograde, mean velocity, and linear flow rate of BDNF-mCherry axonal trafficking into WT, HTT_{SA}, or HTT_{SD} cortical neurons transfected with siCtl or siMecp2, which significantly silenced Mecp2 (n = 3; one-way ANOVA with Tukey's multiple comparisons).

(**F**) Cell viability in WT, HTT_{SA}, or HTT_{SD} neurons transfected with siCtl or siMecp2 measured by MTT assay. No differences were observed between the different groups (n = 2-3; one-way ANOVA Kruskal-Wallis test, p=0.5701)

For all experiments of Fig. 1, we analyzed at least 80 axons and 700 vesicles per condition. Scale bars = 20 µm. *p < 0.05, **p < 0.01, ***p < 0.001, ****p < 0.0001, ns = not significant. Data are presented as the means ± SEM.

Fig. 2. The S421D mutation improves BDNF corticostriatal transport *in vivo*, the motor and autonomic functions of *Mecp2*-deficient mice and increases their lifespan.

(A) The ratio between the striatal and the cortical BDNF determined by quantifying the level of BDNF proteins at the cortex and the striatum of 55 day-old WT (n=8), *Mecp2* KO (n=6),

Mecp2 KO/HTT$_{SD}$ (mimicking the absence of phosphorylation) (n=4) and *Mecp2* KO/HTT$_{SA}$ mice (mimicking constitutive phosphorylation) (n=5). Since striatal BDNF depends only on BDNF transport from the cortex, this ratio reflects BDNF transport through corticostriatal pathway (Mann Whitney test). *p < 0.05, ns = not significant. Data are presented as the means ± SEM.

Quantitative analysis of phospho TrkB protein level in striatum of KO WT mice and KO HTT$_{SD}$ mice by immunoblotting. The relative expression levels of phospho TrkB were normalized against GAPDH and are presented as the ratio. (n = 6 mice per group) (Mann Whitney test; *p < 0.05)

Quantitative analysis of PSD-95 protein level in striatum of *Mecp2* KO/HTT WT mice and KO/HTT$_{SD}$ mice by immunoblotting. The relative expression levels of PSD-95 were normalized against GAPDH and are presented as the ratio. (n = 6 mice per group) (Mann Whitney test; *p < 0.05)

(**B**) *Left:* We investigated the behavior of *Mecp2* KO mice at 35, 45, and 55 days of age and assessed their survival. *Right: Mecp2* KO/HTT$_{SD}$ mice (n = 30) had a significantly longer lifespan than KO (n=22) or KO/HTT$_{SA}$ mice (n = 21) (Kaplan-Meier survival test).

(**C**) Body weight of 10 WT, 24 KO, 32 KO/HTT$_{SD}$, and 24 KO/HTT$_{SA}$ mice at P35 and P55 (one-way ANOVA with Tukey's comparison).

(**D**) Frequency of apnea of 9 WT, 10 KO, 14 KO/HTT$_{SD}$, and nine KO/HTT$_{SA}$ mice at P35 and P55. (Kruskal-Wallis test with Dunn's comparison).

(**E**) *Mecp2* KO/HTT$_{SD}$ mice (n=19) performed as well as WT (n=17) at P35 on the accelerating rotarod test and continued to outperform *Mecp2* KO (n=16) and *Mecp2* KO/ HTT$_{SA}$ (n=13) at P55 (one-way ANOVA with Fisher's LSD test).

(**F**) Time before the onset of spontaneous locomotor activity of 17 WT, 20 KO, 19 KO/HTT$_{SD}$, and 17 KO/HTT$_{SA}$ mice. (Kruskal-Wallis test with Dunn's comparison).

Fig. 3. FK506 restores BDNF axonal transport in Mecp2-silenced axons.

(A) Western blot analysis of DIV 5 cortical neurons transfected with siMecp2 or siControl (siCtl) and treated with 1 μM of FK506 or vehicle for 1 h, and quantification of pS421 HTT (Mann-Whitney). *p < 0.05.

(**B**) Representative kymographs showing axonal trafficking of BDNF-mCherry-containing

vesicles in cortical neurons transfected with siMecp2 or siControl (siCtl) and treated with 1 µM FK506 or vehicle for 1 h. Scale bar = 20 µm.

(**C**) Quantification of anterograde, retrograde, mean velocity, linear flow rate and number of BDNF-mCherry-containing vesicles from the data in (A). Data are presented as the mean ± SEM of at least three independent experiments, with at least 80 axons and 780 vesicles per condition (one-way ANOVA with Tukey's comparison). *p < 0.05, **p < 0.01, ***p < 0.001, ****p < 0.0001, ns = not significant.

Fig. 4. Calcineurin inhibition by FK506 in *Mecp2*-deficient mice improves motor and autonomic functions and extends lifespan through huntingtin-dependent phosphorylation.

(**A**) Western blot of HTT S421 phosphorylation. We treated 30 day-old *Mecp2* KO mice intraperitoneally with FK506 (5 mg/kg) or vehicle and analyzed brain extracts for endogenous HTT phosphorylation by western blotting, 2 h after administration, using an anti-phospho-HTT-S421 specific antibody. The D7F7 antibody recognizes total HTT. (KO FK506 n = 4, KO Vehicle n = 4). The relative protein level of phospho HTT was normalized on total HTT protein level and are presented as the ratio. (Mann Whitney test; *p < 0.05)

(**B-F**) We treated 30 day-old *Mecp2* KO mice (n=10) and *Mecp2* KO/HTT_{SA} mice (n=10) with 5mg/kg FK506 three times a week by intraperitoneal injection and assessed them in various behavioral tests.

(**B**) FK506-treated *Mecp2* KO mice (n = 10) lived longer than vehicle-treated *Mecp2* KO mice (n = 10) and FK506-treated KO HTT_{SA} (n=10) mice (Kaplan-Meier survival test).

(**C**) Body weight of FK506-treated KO, FK506-treated KO HTT_{SA} and vehicle-treated KO mice at P35 and P55. (Mann-Whitney test).

(**D**) Frequency of apnea of FK506-treated KO, FK506-treated KO HTT_{SA} and vehicle-treated KO mice at P35 and P55. (Mann-Whitney test).

(**E**) Motor coordination of FK506-treated, KO FK506-treated KO HTT_{SA} and vehicle-treated KO mice on the accelerating rotarod test at P30 and P50. (Mann-Whitney test).

(**F**) Forelimb strength of FK506-treated, KO FK506-treated KO HTT_{SA} and vehicle-treated KO mice assessed by the grip strength test at P40 and P60. (Mann-Whitney test).

*p < 0.05, **p < 0.01, ns = not significant. Data are means ± SEM.

Fig. EV1 Mecp2 levels and axonal vesicle number in cortical Mecp2-silenced neurons.

(A) Western blot analysis of DIV 5 cortical neurons transfected with siMecp2 or siControl (siCtl) to assess Mecp2 protein levels.

(B) We quantified the number of BDNF-mCherry-containing vesicles trafficking within cortical axons transfected with siMecp2 or siControl (siCtl). Data are presented as the mean ± SEM of at least three independent experiments, with at least 80 axons and 700 vesicles per condition (unpaired t-test).

(C) Brain extracts from WT, WT HTT_{SD} and WT HTT_{SA} mice were analyzed by western blotting for total HTT and phospho-HTT. Quantification of n= 3 samples per genotype did not reveal any significant differences on total HTT. The mutation of HTT S421 into alanine or aspartic acid abrogated the recognition of phospho-HTT by the phospho-specific antibody, further demonstrating the specificity of HTT phosphorylation at S421 (one-way ANOVA test followed by Tukey's post-hoc analysis for multiple comparisons).

(D) We quantified the number of BDNF-mCherry-containing vesicles trafficking within WT, HTT_{SA}, or HTT_{SD} cortical axons. Data are presented as the mean ± SEM of at least three independent experiments, with 80 axons and 700 vesicles per condition (one-way ANOVA test followed by Tukey's post-hoc analysis for multiple comparisons).

(E) Western blot analysis of DIV 5 HTT_{SA} or HTT_{SD} cortical neurons transfected with siMecp2 or siControl (siCtl) to assess Mecp2 protein levels.

(F) Quantification of the number of BDNF-mCherry-containing vesicles trafficking within WT, HTT_{SA}, or HTT_{SD} cortical axons transfected with siMecp2 or siControl (siCtl). Data are presented as the mean ± SEM of at least three independent experiments, with at least 80 axons and 700 vesicles per condition (one-way ANOVA test followed by Tukey's post-hoc analysis for multiple comparisons). ns = not significant.

(G) Representative western blot analysis of PSD-95 and phospho TrkB protein levels in striatum samples from WT, KO HTT_{SD}, KO WT and KO HTT_{SA} mice.

Fig. EV2 Phenotypic characterization of WT, WT HTT_{SD}, WT HTT_{SA} (A, B, C and D) mice and WT, KO HTT_{SD}, KO HTT_{SA} (E, F, G and H) mice.

(A) There were no significant differences in body weight between six-month-old WT, HTT_{SD}, and HTT_{SA} mice. (WT: n = 11; HTT_{SD}: n = 6, and HTT_{SA}: n = 10).

(B) No significant differences in the distance travelled in the open-field between four-month-old WT, HTTSD and HTTSA mice. (WT: n = 10; HTT_{SD}: n = 6 HTT_{SA}: n = 11).

(C) No differences between genotypes in the accelerating Rotarod test for assessing motor coordination of six-month-old WT (n = 11), HTT_{SD} (n = 11) and HTT_{SA} mice (n = 12).

(D) No differences in forelimb strength of six-month-old WT (n = 11), HTT_{SD} (n = 11), and HTT_{SA} mice (n = 12) as assessed by the grip-strength test.

(E) No significant differences in body weight between KO/HTT_{SD} (n = 32), KO/HTT_{SA} (n = 24), and KO mice (n = 24) at different postnatal timepoints.

(F) Distance travelled during the open field test by WT (n = 17), KO (n = 20), KO/HTT_{SD} (n = 19), and KO/HTT_{SA} mice (n = 17) at P35 and P55. Results are expressed in meters.

(G-H) Results of 24-hour Phenorack monitoring to measure the spontaneous activity of 12 WT, 12 KO, 8 KO/HTT_{SD}, and 7 KO/HTT_{SA} mice at P45 (G). Distance travelled at 8 AM versus 8 PM (H). (Kruskal-Wallis test with Dunn's comparison). *p < 0.05, **p < 0.01, ***p < 0.001, ****p < 0.0001, ns = not significant. Data are presented as the means ± SEM.

Fig. EV3 Acute and chronic FK506 treatment of WT, WT HTT_{SA} and Mecp2 KO mice.

(A) Western blot of HTT S421 phosphorylation. We treated WT and WT HTT_{SA} 30 day-old mice intraperitoneally with FK506 (5 mg/kg) or vehicle and analyzed brain extracts for endogenous HTT phosphorylation by western blotting, 2 h after administration (WT FK506 = 3, WT Vehicle = 6, WT HTT_{SA} FK506 = 3, WT HTT_{SA} Vehicle =3). The relative protein level of phospho HTT was normalized on total HTT protein level and are presented as the ratio (Mann Whitney test; *p < 0.05).

(B) Western blot of HTT S421 phosphorylation. We treated WT, WT HTT_{SA} and *Mecp2* KO 30 day-old mice intraperitoneally with FK506 (5 mg/kg) or vehicle chronically for 20 days and analyzed brain extracts for endogenous HTT phosphorylation by western blotting, 2 h after the last administration (KO FK506 n = 2, KO Vehicle n = 2, WT FK506 = 2, WT Vehicle = 2, WT HTT_{SA} FK506 = 2, WT HTT_{SA} Vehicle =2).

(C) Western blot of HTT and Mecp2. We treated WT and *Mecp2* KO 30 day-old mice intraperitoneally with FK506 (5 mg/kg) or vehicle chronically for 20 days (WT FK506 = 3,

WT Vehicle = 3, WT HTT_{SA} FK506 = 3, WT HTT_{SA} Vehicle =3).

Fig. EV4 Absence of cytotoxicity and increasd neuronal activity after chronic FK506 treatment.

(A) FK506 did not increase the levels of cleaved-Caspase 3, as shown by immunostaining. Representative images of Striatum labeled with Casp3 (green) and DAPI of 50-day-old Mecp2 KO mice treated with FK506 (right panel) or vehicle (left panel) for 20 days.

(B) Absence of apoptosis in the dorsal striatum of Mecp2-knockout mice treated chronically with FK505 or with Vehicle. TUNEL assay was used to detect potential apoptotic neurons in 50-day-old Mecp-deficient mice (*n*=3 for each stage). Left panel: detection of cells containing fragmented DNA after desoxyribonuclease I treatment of a representative dorsal striatum section originating from one Mecp2 - knockout and one wild-type animal. No labelled cells were visible after counting all striatum sections of 50-day-old Mecp2 - knockout mice.

(C) FK506 tends to increase the number of c-Fos-positive neurons. Representative images of striatum labeled with cFos (green) of 50 days old KO mice treated with FK506 (right panel) or vehicle (left panel) for 20 days.

Fig. EV5 Breathing patterns in 55-day-old WT, KO Vehicle, KO FK506, KO/HTT_{SD} and KO/HTT_{SA} mice.

On the left: Typical plethysmographic recordings of breathing (inspiration upward) performed in quiet, 55-day-old WT, KO Vehicle, KO FK506, KO/HTT_{SD} and KO/HTT_{SA} mice.

On the right: Distribution of frequency values recorded in WT, KO Vehicle, KO FK506, KO/HTT_{SD} and KO/HTT_{SA} mice. Frequency histograms represent the number of occurrences (ordinate) of breathing frequency during 4 consecutive minutes separated in 0,05-second time windows.

Movie EV1 BDNF vesicle trafficking in axons of cortical Mecp2-silenced neurons.

BDNF-mCherry-containing vesicles trafficking within WT cortical axon transfected with siControl (siCtl) or siMecp2. HTT_{SD} rescues BDNF-mCherry trafficking in siMecp2 cortical axons.

Movie EV2 BDNF vesicle trafficking in axons of cortical Mecp2-silenced neurons treated with FK506.

BDNF-mCherry-containing vesicles trafficking within cortical axons transfected with siMecp2 or siControl (siCtl) and treated with 1 μM FK506 or vehicle for 1 h. FK506 rescues BDNF-mCherry trafficking in siMecp2 cortical axons.

Figure 1

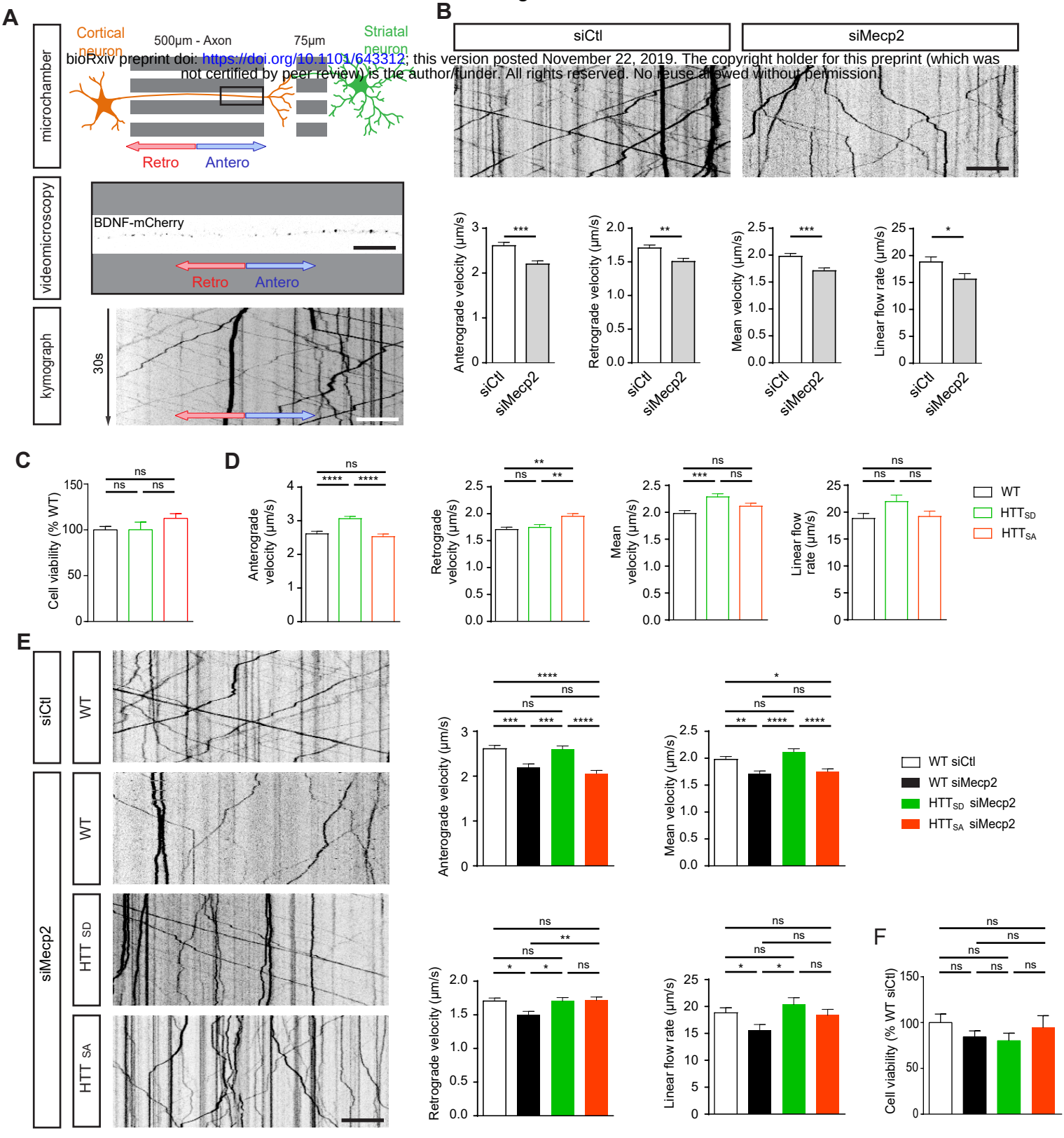

Figure 2

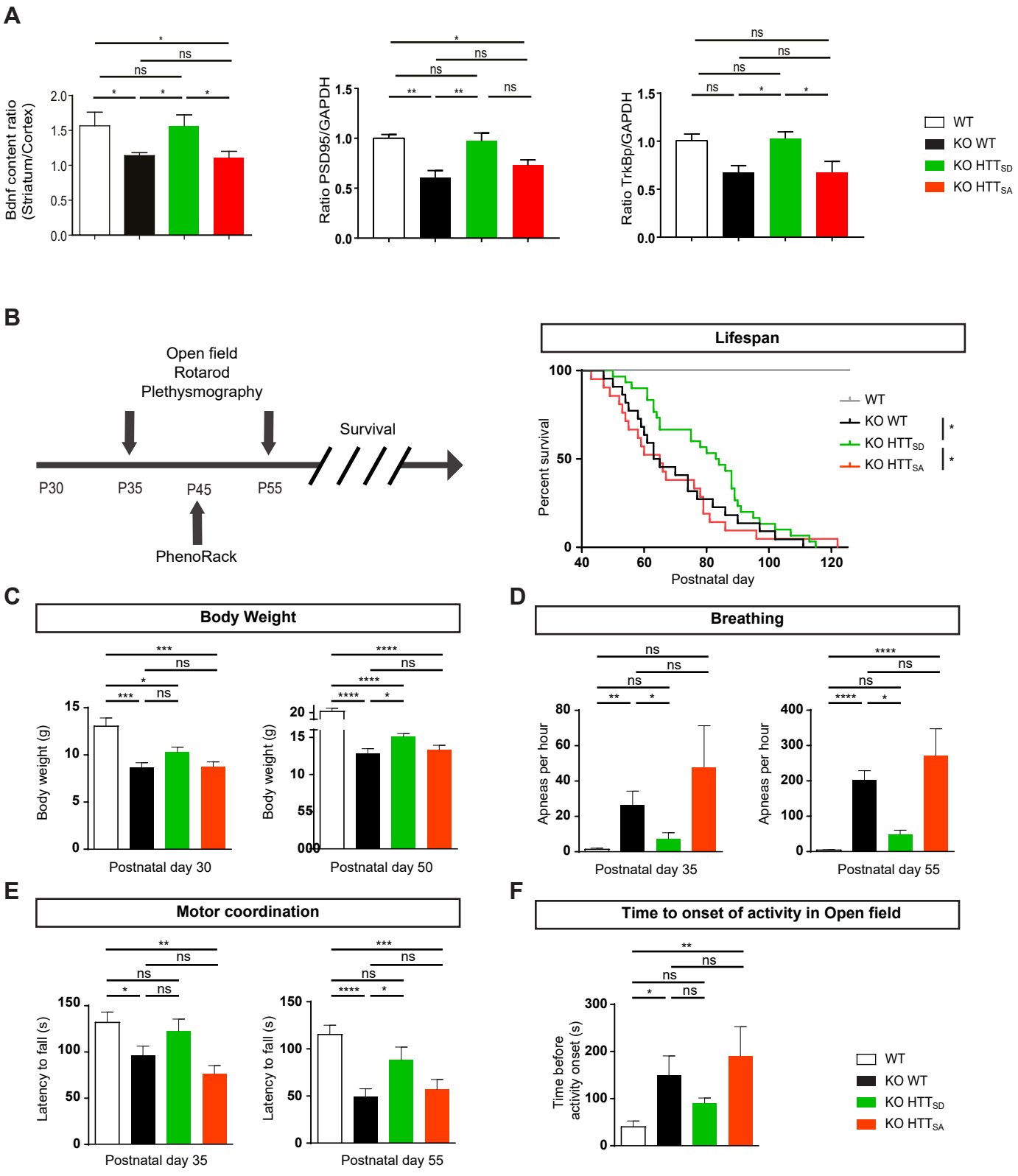

Figure 3

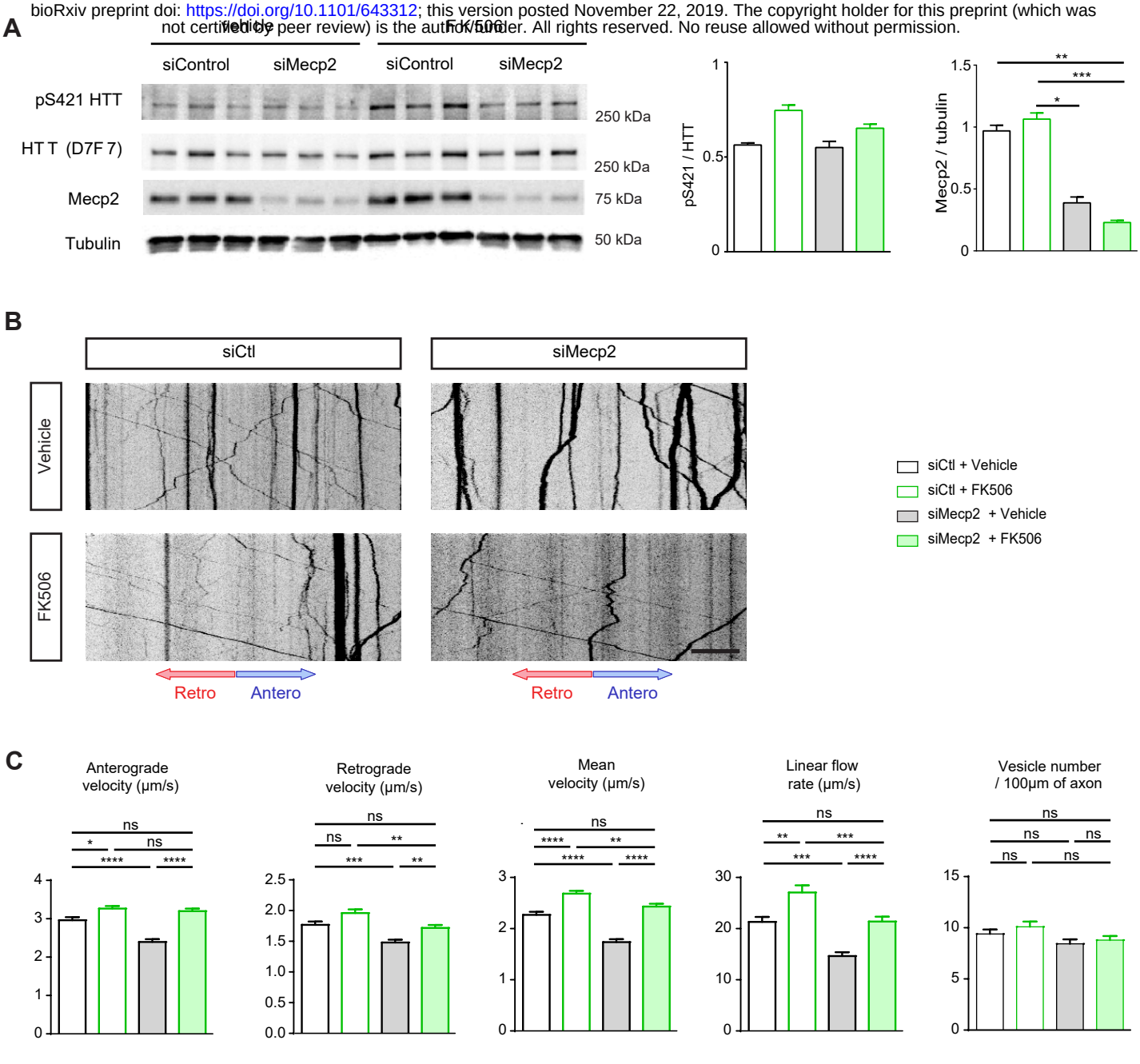

Figure 4

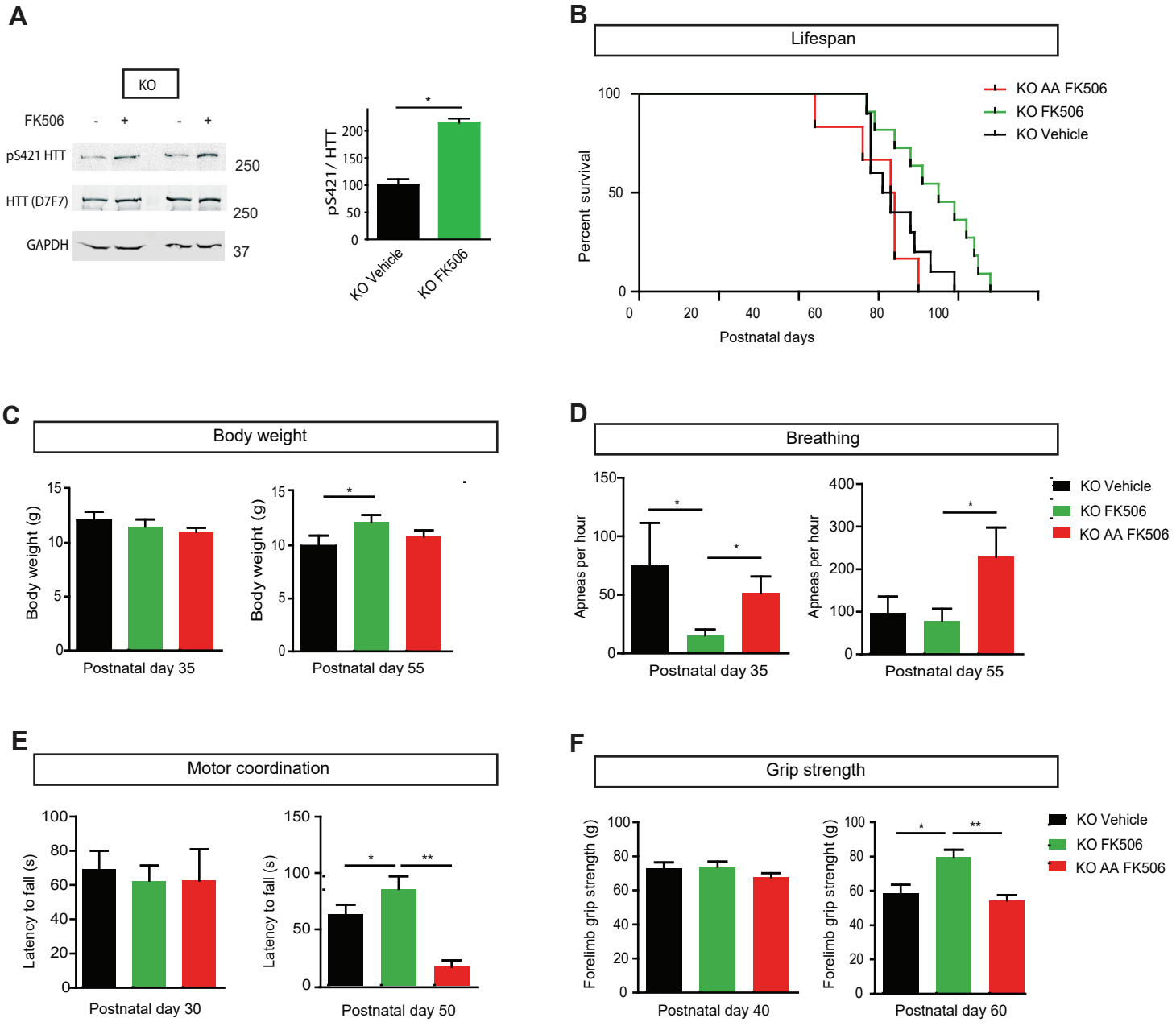

Supplementary Figure 1

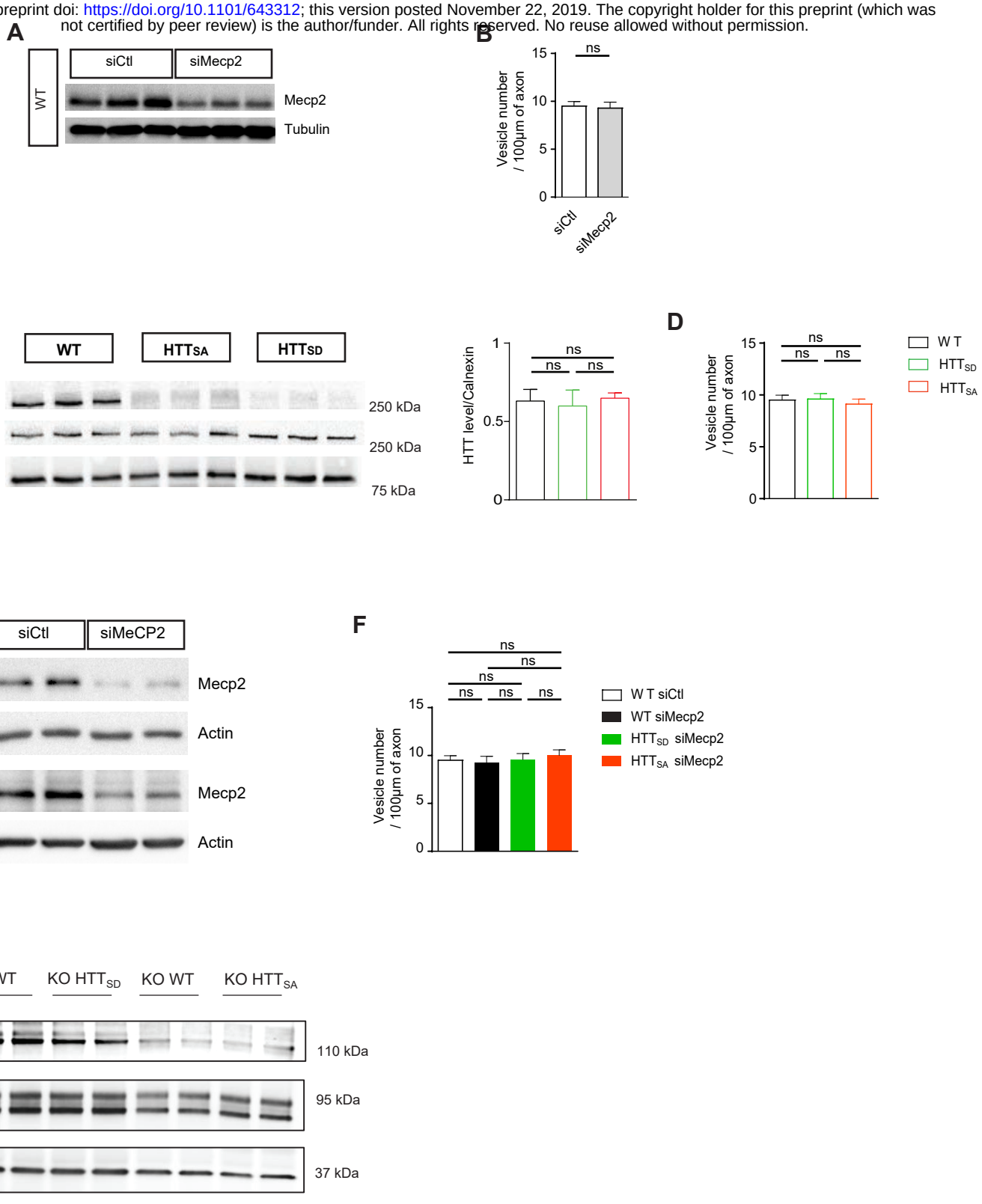

Supplementary Figure 2

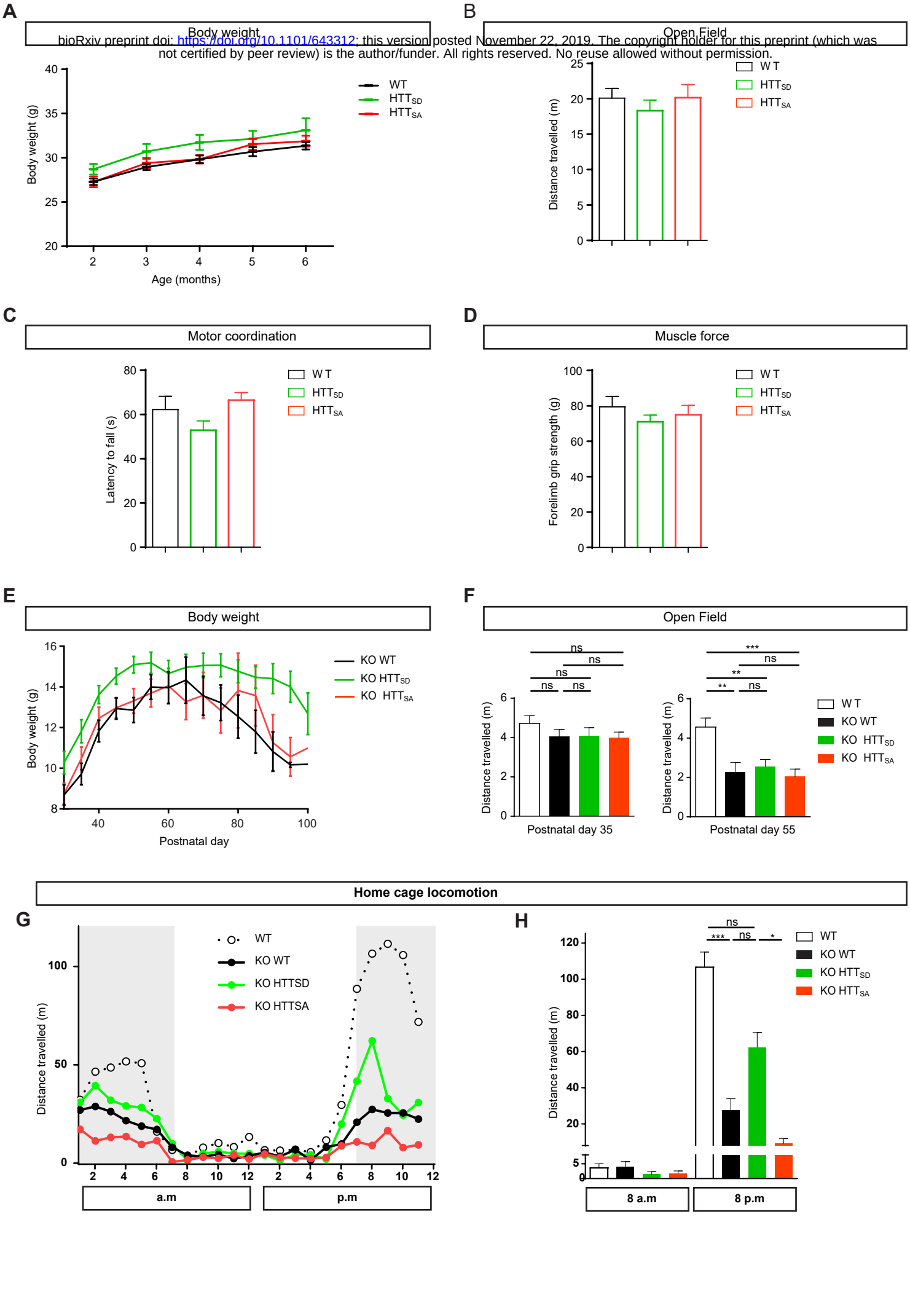

Supplementary Figure 3

A

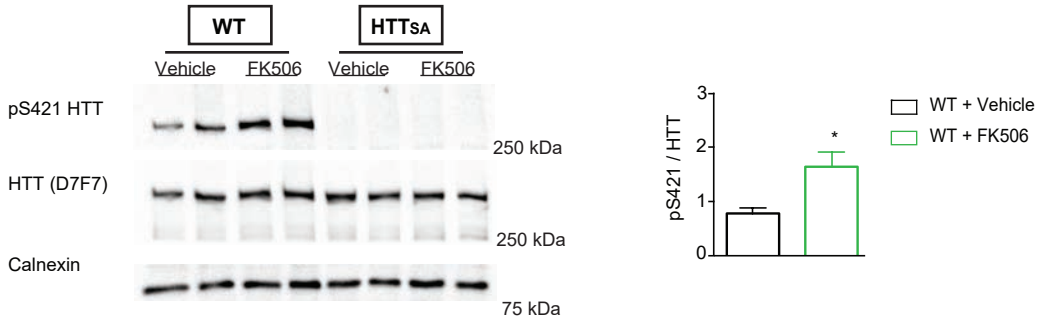

B

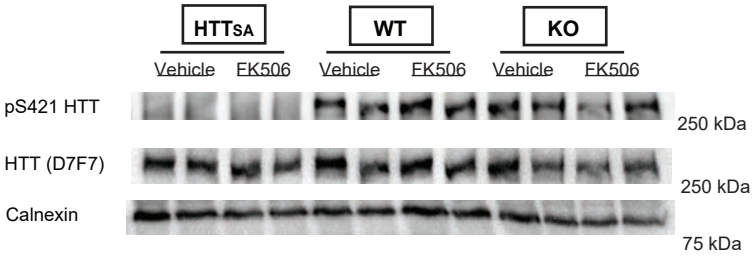

C

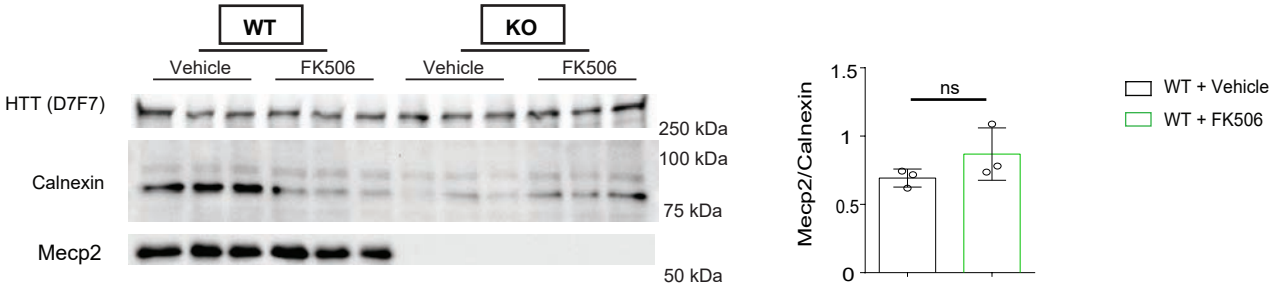

Supplementary Figure 4

A

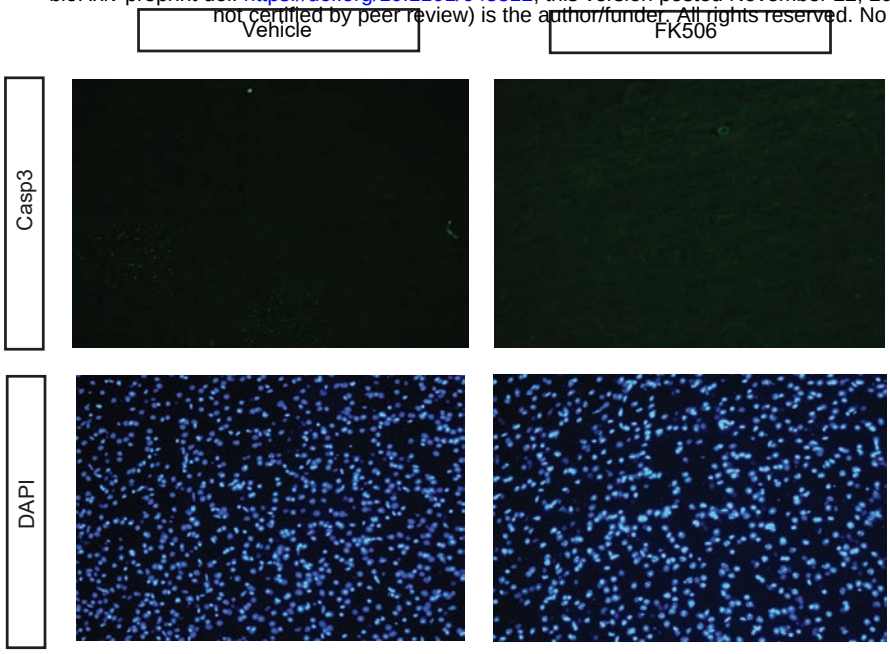

B

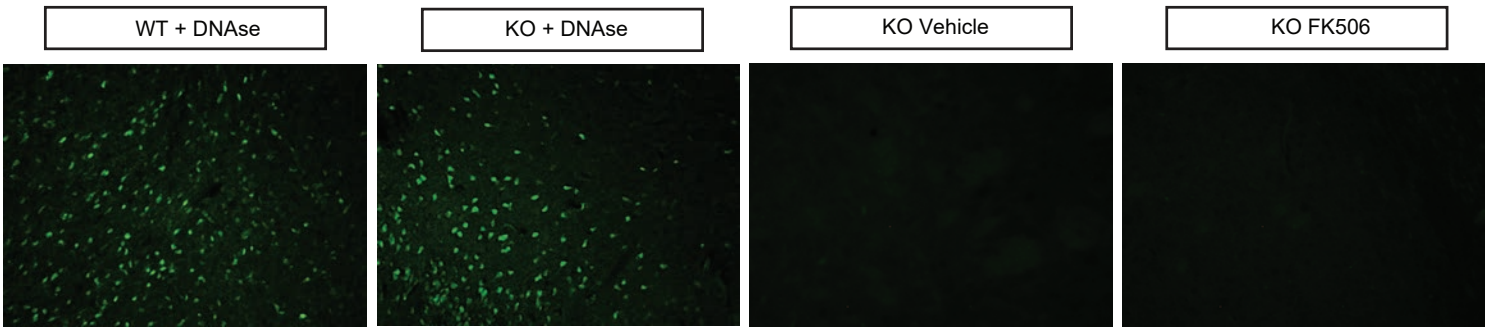

C

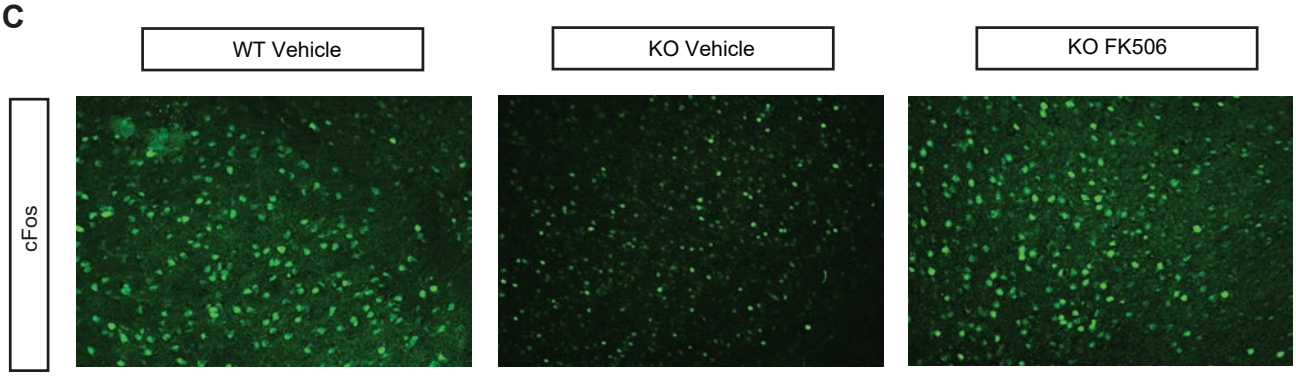

D

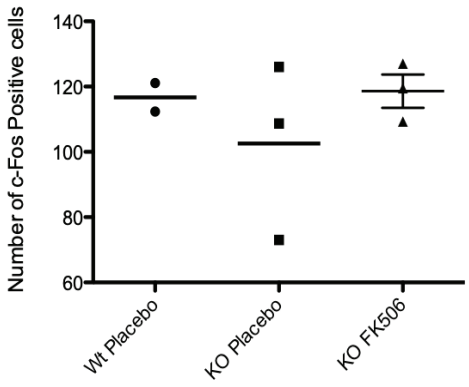

Supplementary Figure 5

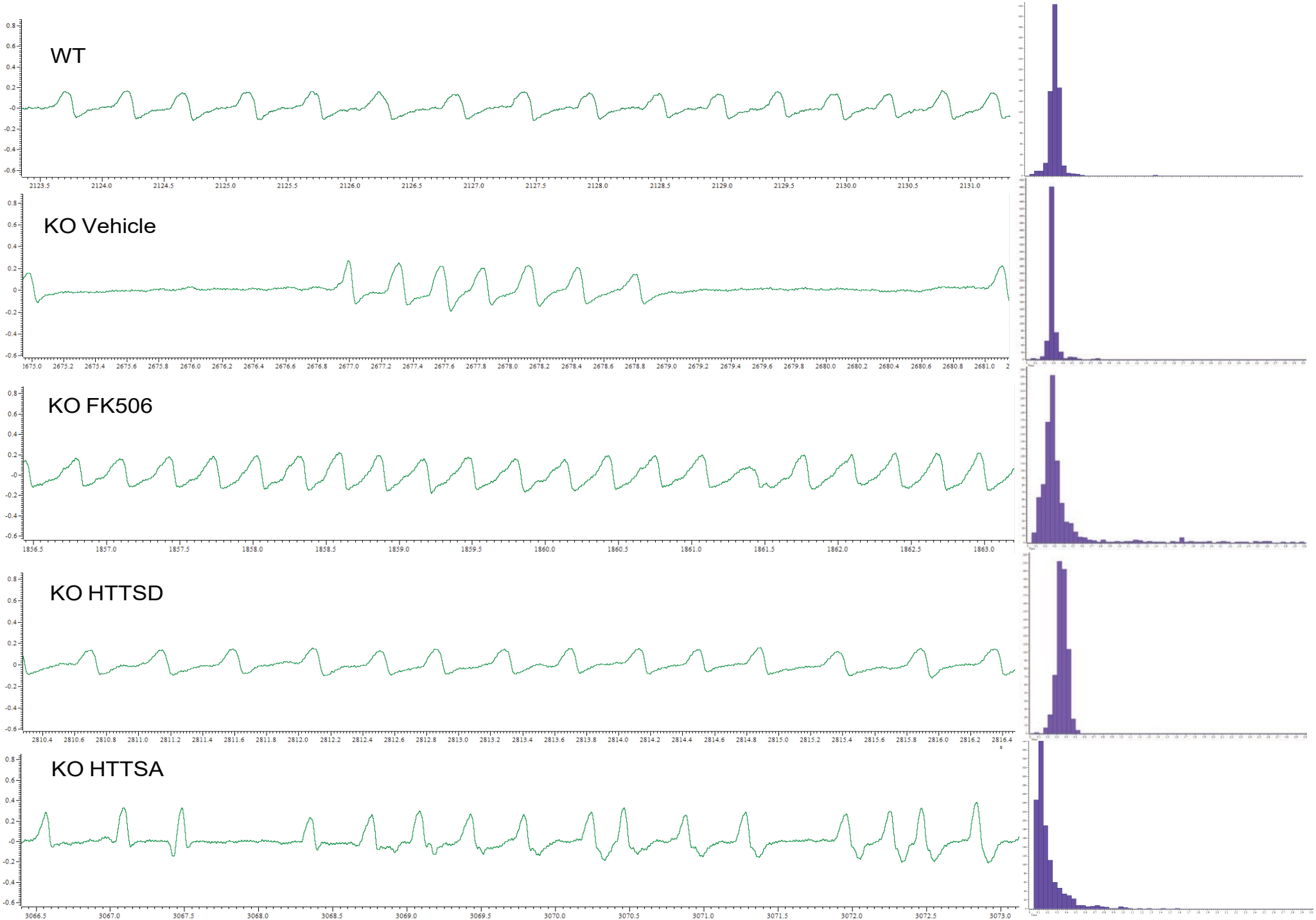

Table S1

	Test	WT (n=11)	HET (n=12)	HET (n=11)
section 1	**In the viewing Jar**			
	Coat color	Normal: 11 (100%)	Normal: 12 (100%)	Normal: 11 (100%)
	Hair length	Normal: 11 (100%)	Normal: 12 (100%)	Normal: 11 (100%)
	Respiration rate	Normal: 11 (100%)	Normal: 12 (100%)	Normal: 11 (100%)
	Tremor	None: 11 (100%)	None: 12 (100%)	None: 11 (100%)
	Body position	Sitting or standing: 11 (100%)	Sitting or standing: 12 (100%)	Sitting or standing: 11 (100%)
	Spontaneous activity	Vigorous scratch, groom, moderate movement: 11 (100%)	Vigorous scratch, groom, moderate movement: 12 (100%)	Vigorous scratch, groom, moderate movement: 11(100%)
	Defecation	None: 10 (91%)	None: 11 (92%)	None: 7 (64%)
		Done: 1 (9%)	Done: 1 (8%)	Done: 4 (36%)
	Urination	None: 11 (100%)	None: 9 (75%)	None: 9 (82%)
		Done: 0 (0%)	Done: 3 (25%)	Done: 2 (18%)
section 2	**In the Arena**			
	Elapsed time before the mouse starts to move (s)	Less than 3s: 11 (100%)	Less than 3s: 12 (100%)	Less than 3s: 11 (100%)
	Transfer arousal	Brief freeze (few sec), then	Brief freeze (few sec), then	Brief freeze (few sec), then
		active movement: 11 (100%)	active movement: 12 (100%)	active movement: 11 (100%)
	Locomotor activity	Average number of squares entered over 1 min exploration: 37 ± 1.859	Average number of squares entered over 1 min exploration: 38.33 ± 1.707	Average number of squares entered over 1 min exploration: 27.55 ± 2.644
	Palpebral Closure	Eyes wide open: 11 (100%)	Eyes wide open: 12 (100%)	Eyes wide open: 11 (100%)
	Piloerection	None: 11 (100%)	None: 12 (100%)	None: 11 (100%)
	Gait	Normal: 11 (100%)	Normal: 11 (92%)	Normal: 11 (100%)
		Fluid but abnormal: 0 (0%)	Fluid but abnormal: 1 (8%)	Fluid but abnormal: 0 (0%)
	Startle Response	Preyer reflex (backwards	Preyer reflex (backwards	Preyer reflex (backwards
		flick of pinnae): 11 (100%)	flick of pinnae): 12 (100%)	flick of pinnae): 11 (100%)
	Pelvic Elevation	Normal (3mm elevation): 11 (100%)	Normal (3mm elevation): 12 (100%)	Normal (3mm elevation): 11 (100%)
	Tail Elevation	Horizontally extended: 11 (100%)	Horizontally extended: 12 (100%)	Horizontally extended: 11 (100%)
	Touch Escape	Mild (escape response	Mild (escape response	Mild (escape response
		to firm stroke):11 (100%)	to firm stroke): 12 (100%)	to firm stroke): 11 (100%)
	Tail morphology	Normal: 11 (100%)	Normal: 12 (100%)	Normal: 10 (91%)
		Kinky: 0 (0%)	Kinky: 0 (0%)	Kinky: 1 (9%)
	Convulsions	Phenotype: 0 (0%)	Phenotype: 0 (0%)	Phenotype: 0 (0%)
section 3	**On or Above the arena**			
	Wire manoeuver (Horizontal bar)	Active grip with hindlegs (5sec): 5 (45%)	Active grip with hindlegs (5sec): 3 (25%)	Active grip with hindlegs (5sec): 2 (18%)
		Difficulty to grasp with hindlegs: 2 (18%)	Difficulty to grasp with hindlegs: 3 (25%)	Difficulty to grasp with hindlegs: 4 (36%)
		Unable to grasp with hindlegs: 1 (9%)	Unable to grasp with hindlegs: 1 (8%)	Unable to grasp with hindlegs: 0 (0%)
		Unable to lift hindlegs, falls within seconds: 3 (27%)	Unable to lift hindlegs, falls within seconds: 5 (42%)	Unable to lift hindlegs, falls within seconds: 5 (45%)
		Falls immediately: 0 (0%)	Falls immediately: 0 (0%)	Falls immediately: 0 (0%)
	Negative geotaxis (vertical grids)	Turns and climbs the grid: 11 (100%)	Turns and climbs the grid: 12 (100%)	Turns and climbs the grid: 11 (100%)
	Positional Passivity : struggles when held by tail	Yes: 11 (100%)	Yes: 12 (100%)	Yes: 11 (100%)
	Trunk curl	Absence: 11 (100%)	Absence: 12 (100%)	Absence: 11 (100%)
	Limb grasping	Present: 11 (100%)	Present: 12 (100%)	Present: 11 (100%)
	Visual Placing	Before vibrasse contact: 11 (100%)	Before vibrasse contact: 12 (100%)	Before vibrasse contact: 11 (100%)
	Grip Strength	Moderate grip, effective: 11 (100%)	Moderate grip, effective: 12 (100%)	Moderate grip, effective: 11 (100%)
	Body Tone	Slight resistance: 11 (100%)	Slight resistance: 12 (100%)	Slight resistance: 11 (100%)
	Head morphology	Normal: 11 (100%)	Normal: 12 (100%)	Normal: 11 (100%)
	Corneal Reflex	Active single eye blink: 11 (100%)	Active single eye blink: 12 (100%)	Active single eye blink: 11 (100%)
section 4	**Supinate restraint**			
	Lacrimation	None: 11 (100%)	None: 12 (100%)	None: 11 (100%)
	Whisker morphology	Normal: 11 (100%)	Normal: 12 (100%)	Normal: 11 (100%)
	Tooth morphology	Normal: 11 (100%)	Normal: 12 (100%)	Normal: 11 (100%)
	Provoked Biting	Present: 11 (100%)	Present: 12 (100%)	Present: 11 (100%)
	Salivation	None: 11 (100%)	None: 12 (100%)	None: 11 (100%)
	Heart Rate	Normal: 11 (100%)	Normal: 12 (100%)	Normal: 11 (100%)
	Abdominal tone	Slight resistance: 11 (100%)	Slight resistance: 12 (100%)	Slight resistance: 11 (100%)
	Skin color	Pink: 11 (100%)	Pink: 12 (100%)	Pink: 11 (100%)
	Toe pinch	Slight withdrawal, not brisk: 0 (0%)	Slight withdrawal, not brisk: 1 (8%)	Slight withdrawal, not brisk: 0 (0%)
		moderate withdrawal, not brisk: 11 (100%)	moderate withdrawal, not brisk: 11 (92%)	moderate withdrawal, not brisk: 11 (100%)